NASA TECHNICAL MEMORANDUM

NASA TM X-2933

NASA TM X-2933

SUMMARY OF STABILITY AND CONTROL CHARACTERISTICS OF THE XB-70 AIRPLANE

by Chester H. Wolowicz and Roxanah B. Yancey

Flight Research Center
Edwards, Calif. 93523

NATIONAL AERONAUTICS AND SPACE ADMINISTRATION • WASHINGTON, D. C. • OCTOBER 1973

1. Report No.	2. Government Accession No.	3. Recipient's Catalog No.
NASA TM X-2933		

4. Title and Subtitle	5. Report Date
SUMMARY OF STABILITY AND CONTROL CHARACTERISTICS OF THE XB-70 AIRPLANE	October 1973
	6. Performing Organization Code

7. Author(s)	8. Performing Organization Report No.
Chester H. Wolowicz and Roxanah B. Yancey	H-781
	10. Work Unit No. 501-06-05-00
9. Performing Organization Name and Address NASA Flight Research Center P. O. Box 273 Edwards, California 93523	11. Contract or Grant No.
	13. Type of Report and Period Covered Technical Memorandum
12. Sponsoring Agency Name and Address National Aeronautics and Space Administration Washington, D. C. 20546	14. Sponsoring Agency Code

15. Supplementary Notes

16. Abstract

The stability and control characteristics of the XB-70 airplane were evaluated for Mach numbers up to 3.0 and altitudes up to 21,300 meters (70,000 feet). The airplane's inherent longitudinal characteristics proved to be generally satisfactory. In the lateral-directional modes, the airplane was characterized by light wheel forces, low static directional stability beyond approximately 2° of sideslip, adverse yaw response to aileron inputs throughout the entire Mach number range, and negative effective dihedral with wingtips full down.

At subsonic Mach numbers, with the flight augmentation control system off, the light wheel forces and adverse yaw response to aileron inputs caused the pilots to minimize use of the ailerons. At supersonic Mach numbers, with the augmentation system off, the adverse yaw due to aileron and the negative effective dihedral were conducive to pilot-induced oscillations. These problems were eliminated by using the augmentation system, except when large aileron inputs were made at Mach numbers near 0.95 with the wingtips undeflected.

The lateral bobweight was found to be highly effective as an auxiliary stabilization device.

17. Key Words (Suggested by Author(s))	18. Distribution Statement
Stability and control XB-70 airplane	Unclassified - Unlimited

19. Security Classif. (of this report)	20. Security Classif. (of this page)	21. No. of Pages	22. Price*
Unclassified	Unclassified	54	Domestic, $3.50 Foreign, $6.00

*For sale by the National Technical Information Service, Springfield, Virginia 22151

SUMMARY OF STABILITY AND CONTROL CHARACTERISTICS OF THE XB-70 AIRPLANE

Chester H. Wolowicz and Roxanah B. Yancey
Flight Research Center

INTRODUCTION

The XB-70 airplane provided valuable full-scale flight data for the advancement of supersonic transport technology because of its size, weight, and performance. A substantial amount of stability and control information was obtained during the first XB-70 performance demonstration tests, which were conducted jointly by the North American Rockwell Corporation and the U.S. Air Force. In the second phase of the program, performed by the National Aeronautics and Space Administration and the Air Force, additional data were obtained in direct support of the advancement of supersonic transport technology. In the demonstration phase of the program, the XB-70-1 airplane was the primary source of data, although data were obtained for both the XB-70-1 and XB-70-2 airplanes. In the second phase of the program, the XB-70-1 airplane was the sole source of data because the XB-70-2 airplane was destroyed in a midair collision before the start of the second phase.

Reference 1 is a preliminary study of the XB-70-1 airplane's stability and control and dynamic characteristics. An assessment of handling qualitites criteria based on preliminary XB-70 flight-test experience is reported in reference 2. Reference 3 gives a detailed account of stability and control problems encountered on the XB-70-1 airplane during an emergency situation resulting from a structural failure at the nacelle apex.

This report summarizes the stability and control characteristics of the XB-70-1 airplane and describes some unusual problems that were encountered with it. Data which have become available only recently are used to explain some of the discrepancies between predictions and flight. The report discusses the airplane's longitudinal characteristics during takeoff and landing, its longitudinal static and dynamic stability and control characteristics for the cruise configuration, and its lateral-directional static and dynamic stability and control characteristics. Several problems that were encountered are discussed, and wherever possible the underlying causes are indicated. Data for the XB-70-2 airplane are used where they effectively illustrate problems common to both airplanes.

SYMBOLS

Data are presented as standard NASA coefficients of forces and moments, which are referred to the body axes passing through the center of gravity. The positive directions are: X, forward; Y, to the right; and Z, down. Positive directions of forces, moments, angular displacements, and velocities are in accord with the right-hand rule.

Although the measurements were taken in the U.S. Customary System of Units, the results are presented in the International System of Units. Equivalent values in U.S. Customary Units are indicated parenthetically. Factors relating the two systems are presented in reference 4.

a_n, a_t — normal and transverse accelerations at the center of gravity, respectively, g

b — wingspan, m (ft)

CAS — calibrated airspeed, knots

C_l — rolling-moment coefficient, $\frac{\text{Rolling moment}}{\bar{q}Sb}$

C_{l_β} — effective dihedral parameter, $\frac{\partial C_l}{\partial \beta}$, per deg

$C_{l_{\delta_a}}$ — roll control derivative, $\frac{\partial C_l}{\partial \delta_a}$, per deg

C_m — pitching-moment coefficient, $\frac{\text{Pitching moment}}{\bar{q}S\bar{c}}$

C_n — yawing-moment coefficient, $\frac{\text{Yawing moment}}{\bar{q}Sb}$

C_{n_β} — static directional stability derivative, $\frac{\partial C_n}{\partial \beta}$, per deg

$C_{n_{\delta_a}} = \frac{\partial C_n}{\partial \delta_a}$, per deg

$\bar{c}$ — mean aerodynamic chord, m (ft)

F_p, F_s, F_w — pedal, stick, and wheel forces, respectively (positive when right pedal is forward, stick is pulled, wheel is turned clockwise), N (lb)

g acceleration of gravity, m/sec^2 (ft/sec^2)

h_p pressure altitude, m (ft)

I_X, I_Y, I_Z moments of inertia about the X-, Y-, and Z-body axes, respectively, $kg\text{-}m^2$ ($slug\text{-}ft^2$)

I_{XZ} product of inertia referred to X- and Z-body axes, $kg\text{-}m^2$ ($slug\text{-}ft^2$)

$$\bar{L}'_\beta = \left(C_{l_\beta} + \frac{I_{XZ}}{I_Z} C_{n_\beta} \right) \frac{\bar{q}Sb}{I_X - \frac{I_{XZ}^2}{I_Z}}, \text{ per sec}^2$$

$$\bar{L}'_{\delta_a} = \left(C_{l_{\delta_a}} + \frac{I_{XZ}}{I_Z} C_{n_{\delta_a}} \right) \frac{\bar{q}Sb}{I_X - \frac{I_{XZ}^2}{I_Z}}, \text{ per sec}^2$$

M Mach number

$$\bar{N}'_\beta = \left(C_{n_\beta} + \frac{I_{XZ}}{I_X} C_{l_\beta} \right) \frac{\bar{q}Sb}{I_Z - \frac{I_{XZ}^2}{I_X}}, \text{ per sec}^2$$

$$\bar{N}'_{\delta_a} = \left(C_{n_{\delta_a}} + \frac{I_{XZ}}{I_X} C_{l_{\delta_a}} \right) \frac{\bar{q}Sb}{I_Z - \frac{I_{XZ}^2}{I_X}}, \text{ per sec}^2$$

P period of damped natural frequency of the airplane, sec

p, q, r rate of change in roll, pitch, and yaw angles, respectively, rad/sec or deg/sec

$\dot{p} = \frac{\partial p}{\partial t}$

$\bar{q}$ dynamic pressure, $0.5\rho V^2$, N/m^2 (lb/ft^2)

S wing area, m^2 (ft^2)

$T_{1/2}$	time required for transient oscillation to damp to half amplitude, sec
t	time, sec
V	airspeed, m/sec (ft/sec)
W	weight, N (lb)
α,β	angle of attack and angle of sideslip, respectively, deg
Δ	increment
$\delta_a,\delta_e,\delta_r$	aileron, elevator, and rudder deflections, respectively (positive when aileron deflection produces right roll, trailing edge of elevator is down, trailing edge of rudder is to the left), deg
$\delta_{a_\beta} = \frac{\partial \delta_a}{\partial \beta}$	
δ_c	canard deflection (positive when leading edge is up), deg
δ_p	pedal deflection (positive when right pedal is forward), cm (in.)
$\delta_{r_\beta} = \frac{\partial \delta_r}{\partial \beta}$	
δ_T	wingtip position, deg
δ_w	wheel displacement, deg
ζ	ratio of actual to critical damping
θ,φ,ψ	Euler angles of pitch, roll, and yaw, respectively, deg
ρ	mass density of air, kg/m^3 ($slug/ft^3$)
ω_d	damped natural frequency, rad/sec
ω_φ	numerator frequency of $\frac{p}{\delta_a}$ response function, rad/sec
$\lvert\ \rvert$	absolute value

Subscripts:

i	indicated
ps	pilot station

DESCRIPTION OF THE AIRPLANE

The XB-70 airplane (fig. 1) was designed for long-range supersonic cruise flight. It had a design gross weight of more than 2,224,100 newtons (500,000 pounds) and a design cruise speed of Mach 3.0 at an altitude of approximately 21,300 meters (70,000 feet). Two airplanes were built that were identical in configuration except that the first airplane (XB-70-1) had zero geometric dihedral and the second airplane (XB-70-2) had 5° of dihedral. The physical characteristics of the XB-70-1 airplane are listed in table 1.

The airplane had a thin, low-aspect-ratio, 65.5° leading-edge delta wing with folding tips. The wingtip deflections with respect to the horizontal plane were the same for both airplanes. The wing had segmented elevons for pitch and roll control and twin movable vertical stabilizers with 45° hinge lines. The variable-incidence canard had trailing-edge flaps. The windshield (figs. 2(a) to 2(c)) could be lowered for greater visibility during takeoff and landing and raised to a streamlined position for cruise flight.

When the wingtips were deflected, the two outermost elevon segments were faired to form a part of the folded tip. The normal operational limits of the three wingtip configurations are indicated in figure 3. At first the normal operating procedure was to fly with the wingtips undeflected up to high subsonic speeds. This procedure was later modified so that the wingtips were deflected 25° shortly after takeoff and 65° at a Mach number of 1.3.

Control System

The XB-70-1 airplane's irreversible control system is described in detail in reference 5. Table 2 lists the maximum displacement, free play, and breakout force of the cockpit control column, wheel, and rudder pedals. Also included in the table are the maximum displacement and rate of travel of the elevons, rudder, canard, and flap.

Longitudinal control.– The canard provided some of the primary pitch control and had a flap for use during takeoff and landing. For normal takeoffs and landings, the forepart of the canard was fixed at 0° incidence and the canard flap was full down at 20°. Except during takeoff and landing, the canard responded to pilot elevator inputs in a ratio of 1 to -6.67. The pitch mode of the flight augmentation control system (FACS) activated the elevator only. For the first phase of the flight-test program, the canard setting was 2.25° when $\delta_e = 0°$. In the second phase of the program (from flight 53 on), the canard setting was 3° when $\delta_e = 0°$.

The force-feel system for the pitch-control column was composed of a bungee spring load, a longitudinal bobweight in the aft portion of the control system, and dynamic pressure bellows ($\bar{q}$ bellows) in the forward portion of the control system.

The pitch mode of the FACS provided stability in Mach number (speed stability), pitch velocity, and normal acceleration. The system had an elevator authority of $\pm 7.5^\circ$ and a filter circuit with a time constant of 0.1 second to reduce undesirable effects due to body bending. In the pitch mode the augmentation system actuated only the elevator mode of the elevons; it did not affect the position of the canard.

A Mach number trim loop was included to provide a positive column force gradient for speed changes because of predicted negative speed stability at high supersonic Mach numbers. This loop sensed Mach number and Mach number rate. The Mach number signal required the pilot to push the column forward to increase speed and pull the column back to reduce speed. The Mach number rate signal provided phugoid damping.

Roll control.- A wheel force-feel system was provided by overcentering compression springs. The wheel force gradient was of the order of 2.49 newtons (0.56 pound) per degree of wheel displacement. (Before flight 8, $\frac{F_w}{\delta_w} = 1.245$ N/deg (0.28 lb/deg).) The lateral trim command produced surface deflection that was proportional to trim knob displacement.

The roll mode of the augmentation system provided roll rate damping. The roll system had an authority of $\pm 15^\circ$ differential aileron, and the gain was fixed. The system contained a loop to provide maneuver control. When roll rate was commanded by the pilot through the primary control system, the loop provided additional roll rate to compensate for the roll damper inputs.

Directional control.- For the landing-gear-up and -extended configurations, the maximum rudder movements were $\pm 3^\circ$ and $\pm 12^\circ$, respectively. Pedal travel was dependent upon the fore and aft pedal adjustment selected by the pilot. The travel was 8.9 centimeters (3.5 inches) with the pedals set full forward and 10.2 centimeters (4.0 inches) with the pedals set full aft. The pedal force-feel system consisted of a pneumatic bungee in the cockpit for braking action on the ground and a spring-loaded bungee in the aft area for pedal force feel in flight. The pedal force per unit of rudder deflection was constant, and the force per unit of pedal displacement was a function of pedal adjustment.

The yaw mode of the augmentation system provided damping for yaw rate. With the gear down, the yaw damper had a rudder authority of $\pm 2^\circ$; with the gear up, the damper authority was $\pm 0.5^\circ$. The augmentation signal was fed to a 3-second washout circuit to minimize turn effects.

Lateral bobweight.- To compensate for a predicted deficiency in effective dihedral on the XB-70-1 airplane, a lateral bobweight was installed on the airplane. It was meant to be used above Mach numbers of 2.6 to minimize the possibility of large

lateral-directional excursions should the augmentation system become inoperative. This system consisted of a spring-centered weight mounted so that it sensed lateral linear acceleration and deflected the elevons proportionately. The result was an induced rolling velocity proportional to sideslip. The bobweight could also be used in conjunction with the augmentation system.

Propulsion System

Propulsion was provided by six YJ93-GE-3 engines equipped with afterburners. Each engine produced 133,400 newtons (30,000 pounds) of thrust at sea level. The engines were mounted side by side under the rear portion of the center section of the wing. There were two two-dimensional, mixed-compression air intake inlets. The position of the inlet ramps could be varied to provide the proper throat area for optimum performance throughout the flight envelope.

Both air intake ducts, which contained three engines each, were equipped with six inlet air bypass doors. The bypass doors were on top of each duct just forward and inboard of the leading edge of the vertical stabilizer (fig. 1). These doors permitted excess inlet air to spill over the top of the wing. They were manually controlled on the XB-70-1 airplane so that the position of the normal shock in the throat of each inlet duct could be varied according to a Mach number schedule. On the XB-70-2 airplane, the doors could be controlled either manually or automatically.

Symmetrical deflection of the bypass doors caused changes in pitch trim and lift (ref. 6). A differential in the left and right inlet throat areas was normally accompanied by a differential in the left and right bypass door openings, and this caused some changes in the airplane's lateral-directional characteristics (ref. 6).

INSTRUMENTATION

The instrumentation pertinent to this report is listed in table 3. Included in the table are the accuracy, transducer range, and sampling rate of the sensor signals.

The Euler attitude, angular rate, and linear and angular acceleration sensors were approximately 5.2 meters (17 feet) forward of the 25-percent chord of the mean aerodynamic chord and alined to within 0.5° of the body axes.

The α- and β-vanes were mounted on the nose boom 91.4 centimeters and 17.8 centimeters (35 inches and 7 inches) in front of the nose of the airplane, respectively.

A pulse code modulation system was used to process the sensed parameters. The system recorded the analog signals from the sensors in digital form on tape on a time-sharing basis.

ANALYSIS OF LONGITUDINAL TRIM AND SIDESLIP DATA

Although most of this report deals with stability and control characteristics and utilizes time histories of the airplane's motions, data are also presented for longitudinal elevator trim settings and lateral-directional static parameters with respect to Mach number, altitude, weight, and center of gravity. Since weight and center of gravity significantly affected elevator trim settings, the flight trim data were normalized to a midweight of 1,645,800 newtons (370,000 pounds) and a midcenter of gravity of $0.222\bar{c}$ when they were compared with predicted trim settings as a function of Mach number and altitude. The selection of these normalized values was influenced by the format of the manufacturer's predictions (ref. 7) and the magnitude of the correction from the normalizing process.

The flight-determined longitudinal trim settings for 1g conditions were normalized by using reference 7 to determine the predicted trim settings for both the normalized and the flight weight and center-of-gravity conditions. The differences in trim thus obtained were applied to normalize the flight data.

The lateral-directional static parameters were obtained from sideslip maneuvers performed with the augmentation system on. Maneuvers flown with the augmentation system off were erratic and thus usually could not be analyzed. Wings-level and constant-heading sideslips produced results that were the same for all practical purposes. The sideslip parameters obtained included the apparent directional stability, δ_{r_β}, the apparent effective dihedral, δ_{a_β}, and the control force parameters $\frac{\Delta F_p}{\Delta \delta_r}$ and $\frac{\Delta F_w}{\Delta \delta_a}$.

DISCUSSION

Longitudinal Characteristics

The airplane's inherent longitudinal stability and control characteristics were generally satisfactory. One problem encountered involved available elevator during landing and another, the significant difference between predicted and flight elevator trim positions at high supersonic speeds. A third problem evolved during the pilot's attempt to control altitude precisely during speed or power changes at high supersonic Mach numbers.

Takeoff.- During the first four flights, the longitudinal bobweight was near the pilot's station. At this location it was subject to excitation during taxi and takeoff by the first wing-fuselage symmetric bending mode of vibration. This excitation caused objectionable elevator inputs and feedback to the control column. The problem was alleviated by relocating the bobweight 8.02 meters (26.34 feet) aft of the $0.222\bar{c}$ center-of-gravity position.

For takeoff the forepart of the canard was fixed at 0° incidence with the canard flap in the full down position (20°). This flap setting increased the down elevator

angle for trim and thus provided a higher trimmed lift capability for takeoff and landing.

A typical takeoff time history is shown in figure 4. In this takeoff, rotation was started at 190 knots, using 8° up elevator. Lift-off took place at an airspeed of 215 knots, followed by gear retraction and a subsequent 10° down elevator setting for trim. Flap retraction resulted in a 7.5° trim change (from 10.5° to 3°). After airspeed increased to approximately 300 knots, the wingtips were deflected 25°. In general, there were no problems in controlling the aircraft during this phase of the flight.

The large change in pitching moment during flap retraction was countered by using the pitch trim switch as well as the control column. Figure 5 shows a time history of a typical canard flap retraction in which the pitch trim switch was activated in small steps (see δ_e trace) to keep the maximum stick force below 90 newtons (20 pounds). In this instance the trim change resulted in approximately 8° of change in elevator angle (from 12° to approximately 4°).

The procedure for deflecting the wingtips from 0° to 25° was similar to that used for retracting the flaps. The trim switch as well as the control column was used to maintain control. The column forces and trim changes during wingtip deflection were much smaller than those experienced during flap retraction.

Landing.– Landing approaches tended to be consistent, that is, they usually had a glide slope between 2° and 2.5°, an airspeed of approximately 200 knots, and an angle of attack of approximately 8°. A typical landing time history is shown in figure 6. In a normal flaps-down approach at lightweight conditions with the center of gravity between $0.233\bar{c}$ and $0.240\bar{c}$, a down elevator position from 11° to 14° was required for trim, as indicated by figure 7. This range was approximately 4° higher than predicted. During one approach, at a landing weight of 1,223,300 newtons (275,000 pounds) and with the center of gravity equal to $0.238\bar{c}$, the elevator trim setting reached the maximum down travel limit of 15°. As a result of this approach, the maximum elevator travel was changed from -25° and 15° to ±20° to provide a margin for trimming and maneuvering.

Several landings were made without the flaps deflected as a result of flap system failures. A time history of one such landing is shown in figure 8. As would be expected, much less down elevator (approximately 3°) was required for the flaps-up landing than for the flaps-down landing for essentially the same weight and center of gravity (figs. 8 and 6). With the flaps up, the approach speed was normally approximately 10 knots faster than with the flaps down.

Longitudinal trim.– The variation of elevator trim setting with Mach number during flight tests at various constant-altitude conditions is shown for three wingtip configurations in figures 9(a) to 9(c). The results are presented for normalized weight and center-of-gravity conditions of 1,645,800 newtons (370,000 pounds) and $0.222\bar{c}$, respectively. Included in the figures are the predicted variations obtained from reference 7.

With the wingtips up and the gear and flaps extended (fig. 9(a)), the flight data show approximately 4° more down elevator for trim than predicted. With gear and flaps

retracted, the flight data for the 0° and 25° wingtip deflections (figs. 9(a) and 9(b)) correlate reasonably well with the predictions for Mach numbers near 0.9. On both sides of this Mach number, the correlation deteriorates. Flight results show approximately 5° to 6° more down elevator than predicted for trim at a Mach number of 1.1. In addition, the flight data in this transonic region show much more speed stability (that is, more positive values for $\frac{\Delta\delta_e}{\Delta M}$) than predicted.

With the wingtips in the full down position, 65° (fig. 9(c)), the least trim discrepancy exists between the flight and predicted results for Mach numbers from 1.4 to 1.8 at the lowest test altitude. The speed stability for all altitudes for which flight data were available correlates well with predictions in this Mach number range. Above a Mach number of 1.8, the discrepancy in trim between flight data and predictions increased with increasing Mach number as well as increasing altitude, and the flight data showed positive speed stability instead of the predicted negative stability. Between Mach numbers of 2.6 and 3.0, the discrepancy was of the order of 10°, with greater flight trim angles than predicted in the downward direction. Because of the positive speed stability, the Mach number trim loop in the control system was not used.

The discrepancies between flight and predicted longitudinal trim were investigated in reference 8, in which flight-measured and predicted longitudinal stability and control characteristics are compared for six flight conditions. The discrepancies were attributed to several factors. The predictions for the airplane were based on tests of a wind-tunnel model equipped with nonsegmented elevons containing strain gages on one side for hinge-moment determination. The use of nonsegmented-elevon data, which were also affected by free play and elasticity in the strain gages, contributed significantly to the discrepancies. In addition, although the gearing between the canard and elevator in the actual airplane was according to design, the predicted canard incidence setting for any one elevator position differed from the incidence setting obtained in flight. Finally, it was difficult to obtain accurate elevator trim settings from model data at supersonic speeds. Reference 8 indicates that this was one of the more significant sources of discrepancy. At a Mach number of 2.5, for example, $\Delta C_m = 0.0007$ was equivalent to 1° of (geared) elevon deflection. Such small values of ΔC_m are easily lost in wind-tunnel testing and plotting accuracy unless great care is taken.

Longitudinal control. – Longitudinal control, which was exercised in such maneuvers as retrimming the airplane following a change in altitude or speed, or both, presented no problems, although more pilot concentration was necessary at the higher supersonic Mach numbers to avoid undesirable changes in altitude. During the early phase of the flight-test program, inadequacies in the pilot's display contributed to this need for greater pilot concentration. One deficiency was the low resolution of the attitude display, which the pilots used for altitude control. A 0.076-centimeter (0.03-inch) deflection of the attitude indicator corresponded to a 1° change in attitude, which at a Mach number of 3.0 resulted in a 914 m/min (3000 ft/min) rate of climb. This 1° change in pitch attitude was hardly discernible on the display, and, as a result, considerable pilot concentration was necessary to fly the airplane at constant altitude. The problem was alleviated to some extent by an improved attitude sensor and a more sensitive display in which the resolution was

increased from 0.076 centimeter to 0.152 centimeter (0.03 inch to 0.06 inch) deflection per degree of change in pitch attitude.

Altitude excursions.– The occurrence of random excursions in indicated altitude at high supersonic speeds suggested that improvements were also needed in the altitude and rate-of-climb sensors. The altitude and rate-of-climb instruments were pressure-sensitive, and they were therefore subject to change as the airplane moved through regions of varying atmospheric pressure at high speeds. The problem was complicated by significant lag in these changes. The absence of corroborative sensors not subject to pressure variations, such as inertial sensors, made it difficult for the pilot to hold altitude. Changes of this nature, although not initially identified as such, were encountered during three different flights of the XB-70-2 airplane during December and January at Mach numbers above 2.6. The same pilot was involved in the three flights. On each flight the pilot reported an altitude excursion on the basis of cockpit altimeter readings. These occurrences were random in time and direction, and varied in magnitude from approximately 91.4 meters to 244 meters (300 feet to 800 feet). In each instance the nose ramp was up and the FACS was on.

A time history of one of the more easily controlled excursions of the eight encountered during one of the flights is shown in figure 10. The airplane was cruising at a pressure altitude of 20,750 meters (68,060 feet) at a Mach number of 2.8 and near 1g level flight conditions. At $t = 10$ seconds, the pilot noted an increasing rate of descent on the altimeter. The corrective control that was applied to arrest the indicated descent was immediately followed by an indicated ascent. Further corrective action over a period of approximately 12 seconds arrested the indicated ascent, and the airplane returned to the normal cruise condition.

During this excursion, a lack of correlation between the control inputs and the responses of the airplane as indicated by the instruments gave the pilot the impression that the airplane was not responding properly. On each following XB-70-2 flight during which excursions were encountered (flights 16 to 18), however, the pilot had the opportunity to make observations, experiment with aircraft behavior, and develop countermeasures. It was finally determined that the indicated excursions were due to atmospheric pressure variations which are normally encountered in a turbulent winter. In trying to take corrective action, the pilot was in effect chasing the indicated pressure altitude. The excursion problem was alleviated to some extent by using a Machmeter and a more sensitive attitude indicator. It should be noted that in another more recent program, a pilot flying an airplane equipped with inertial sensors at a high supersonic Mach number had no difficulty in maintaining altitude when he encountered similar atmospheric pressure variations.

Dynamic stability.– The airplane's unaugmented short-period dynamics are shown in figures 11(a) to 11(c) (from ref. 1) for the flight-test conditions listed in table 4. This figure indicates the correlation between flight data and predicted results to be generally good. The damping ratios show heavy damping of the order of 0.5 and greater in the subsonic region and light damping of the order of 0.10 to 0.15 in the high supersonic region. Heavier damping would have been desirable at high supersonic Mach numbers to make it easier to trim the airplane during a speed or power change. The pitch augmentation system did increase damping to some extent.

Effects of pitch augmentation.– Although the pitch augmentation system enhanced the short-period damping of the airplane in the subsonic Mach number region, the inherently high unaugmented damping gave the pilot a feeling of deadbeat response to longitudinal disturbances. The time histories in figure 12(a) show the small effect of the pitch augmentation system in damping longitudinal pulses at a Mach number of 0.80.

At high supersonic speeds, where the inherent damping was light, the use of the pitch augmentation system was required to minimize pilot workload. The time histories in figure 12(b) show the magnitude of the additional damping provided by the pitch augmentation system at a Mach number of 2.50. Although the augmentation system improves the damping, the pitch response is not deadbeat.

Lateral-Directional Characteristics

With the FACS on, the airplane was generally easy to handle, although the wheel force gradient, $\frac{\Delta F_w}{\Delta \delta_w}$, was considered to be too light. Flight tests with the FACS off revealed several stability and control deficiencies. These deficiencies were the result of a combination of powerful roll control, $C_{l_{\delta_a}}$, limited linear range of static directional stability, C_{n_β}, negative effective dihedral with the wingtips full down at Mach numbers greater than 1, and adverse yaw for all wingtip configurations. Light wheel forces also contributed to the flight control problems resulting from these deficiencies.

The pilots learned how to minimize these problems as they became more familiar with the airplane. However, several of the deficiencies contributed to an unusual stability and control situation during an emergency deceleration and descent due to engine damage. A comprehensive treatment of this incident is given in reference 3.

Landing approach.– In the landing configuration, light wheel forces, powerful roll control, and adverse aileron yaw resulted in highly sensitive lateral-directional control. Because of the highly sensitive roll control and the highly positive effective dihedral, the roll FACS was normally kept on during the landing approach. Although adverse aileron yaw was present, the yaw FACS was usually disengaged to eliminate objectionable feedback to the rudder pedals.

At the beginning of the flight-test program, the pilots tended to overcontrol the airplane in roll and thereby induce lateral disturbances. The time history of a typical case is shown in figure 13. The time history shows that the pilot first applied left aileron to counter a right roll trend. This action induced negative sideslip due to adverse aileron yaw, which in turn tended to counter the left aileron response as a result of the positive dihedral effect. The rest of the time history reflects the tendency of the pilot to overcontrol in roll due to the combined effects of adverse aileron yaw, high positive dihedral, and high aileron and rudder control power. The saw-toothed nature of the φ, p, and β traces is the result of pilot aileron inputs, which were frequently in conflict with the maneuver control loop in the roll FACS.

This loop, as explained in the description of the control system, provided additional roll rate when roll rate was commanded through pilot inputs to compensate for the roll damper inputs.

Static stability.- The static lateral-directional stability characteristics of the airplane obtained from sideslip maneuvers are summarized in figure 14 for various flight-test conditions. The results are presented in the form of apparent directional stability, δ_{r_β}, and apparent effective dihedral, δ_{a_β}, and are compared with corresponding predicted characteristics.

Positive apparent directional stability, δ_{r_β}, is evident for all wingtip configurations. The flight values are generally slightly lower than predicted for the transonic and supersonic Mach number regions. The flight values of apparent effective dihedral, δ_{a_β}, for these Mach numbers are slightly less positive than predicted with the wingtips at 0° and 25°, and significantly more negative than predicted with the wingtips at 65°.

The large difference between the flight and predicted apparent effective dihedral with the wingtips at 65° is due primarily to corresponding differences in C_{l_β} and $C_{n_{\delta_a}}$. Reference 1 shows the flight results for $C_{n_{\delta_a}}$ to be negative for Mach numbers greater than 0.92, whereas the predicted values are positive. The same reference shows C_{l_β} from flight to be less positive than predicted with the wingtips at 25° and more negative than predicted with the wingtips at 65°.

Static control.- The static lateral-directional control characteristics of the airplane, as obtained from sideslip maneuvers, are shown in figure 15. Early in the flight program the wheel force gradient, $\frac{\Delta F_w}{\Delta \delta_w}$, was so light that it caused inadvertent aileron inputs by the pilot. In addition, the side forces due to sideslip were so low in magnitude that they were not apparent to the pilot, making a sideslip indicator necessary to control or eliminate sideslip. These two factors contributed to the occasional but unintentional buildup of excessive sideslip. In addition, the wheel force gradients were not in harmony with the pitch control force gradients. To minimize inadvertent or excessive aileron inputs and to improve control harmony, the design wheel force gradient in roll was doubled in the artificial feel system from 1.245 N/deg (0.28 lb/deg) to 2.49 N/deg (0.56 lb/deg). This change corresponds to an increase in $\frac{\Delta F_w}{\Delta \delta_a}$ from 3.33 N/deg (0.75 lb/deg) to 6.66 N/deg (1.50 lb/deg). Figure 15 shows that the flight values of $\frac{\Delta F_w}{\Delta \delta_a}$ correspond well with the increased design values except above a Mach number of 2.4, where the flight values are lower than predicted.

The flight-determined variation of pedal force with rudder displacement, $\frac{\Delta F_p}{\Delta \delta_r}$, is less than predicted. With consideration for the scatter in the flight data, the mean value of $\frac{\Delta F_p}{\Delta \delta_r}$ is of the order of 120 N/deg (27 lb/deg), as compared with a predicted level of 142 N/deg (32 lb/deg). The discrepancy is attributed primarily to elasticity in the rudder actuators. This elasticity caused slight displacements of the rudders about their hinge lines in addition to the pedal-induced displacements because of inertial and aerodynamic loads. These effects are discussed in greater detail in the Dutch-roll characteristics section (page 15).

The differences between flight and predicted values of $\frac{\Delta F_p}{\Delta \beta}$ and $\frac{\Delta F_w}{\Delta \beta}$ reflect discrepancies in $\frac{\Delta F_p}{\Delta \delta_r}$ and $\frac{\Delta \delta_r}{\Delta \beta}$ and $\frac{\Delta F_w}{\Delta \delta_a}$ and $\frac{\Delta \delta_a}{\Delta \beta}$, respectively. Although the pilots made no adverse comments concerning pedal force, they considered the wheel force variation with sideslip to be highly sensitive, particularly under conditions of high roll control effectiveness, $C_{l_{\delta_a}}$, adverse aileron yaw (negative $C_{n_{\delta_a}}$), and high $\frac{\Delta \varphi}{\Delta \psi}$ ratio.

Handling problems during sideslips.- Sideslip maneuvers in the clean configuration were adversely affected by a drop in static directional stability, C_{n_β}, at sideslip angles greater than approximately 2° for all Mach numbers and wingtip configurations. At Mach numbers greater than 0.92, adverse aileron yaw (negative $C_{n_{\delta_a}}$) for all wingtip configurations and negative effective dihedral (positive C_{l_β}) with the wingtips full down also contributed to the difficulty of performing sideslip maneuvers.

Because of the deterioration in directional stability, C_{n_β}, the previously discussed flight-determined apparent directional stability, δ_{r_β}, apparent effective dihedral, δ_{a_β}, and sideslip force gradients, $\frac{\Delta F_w}{\Delta \beta}$ and $\frac{\Delta F_p}{\Delta \beta}$, are valid only for the sideslip range from approximately ±1.5° to ±2.0°. The deterioration in directional stability is evident in figures 16(a) and 16(b), which show results from a sideslip maneuver with the FACS engaged. The deterioration is due to the action of the canard tip vortices that pass between the vertical tails, and, as indicated in figures 17(a) and 17(b), it is primarily a function of angle of attack, with Mach number as a contributing factor. The data in this figure were obtained from unpublished results of rigid model tests in the Ames Research Center's 11-Foot Transonic Wind Tunnel.

Adverse yaw due to aileron (negative $C_{n_{\delta_a}}$) occurred at Mach numbers greater than 0.92 and proved to be a nuisance factor during most routine operations. While preparing for the flight program, the pilots became accustomed to simulated handling characteristics which were based on positive values of $C_{n_{\delta_a}}$. As a result, the pilot for the first transonic flight experienced a sideslip excursion which was erroneously attributed to inadequate directional stability. The time history of this encounter, which occurred at a Mach number of 1.07 with the wingtips up and the FACS off, is shown in figure 18. The pilot deliberately induced a sideslip of 1°. Unaware of the adverse yaw action of the ailerons, he then reduced the rudder input for recovery. As a result of the accompanying aileron input, the sideslip continued to increase. Recovery was eventually accomplished by reducing the aileron input. After the real cause of the sideslip excursion became known, the pilots used the ailerons cautiously and sparingly.

Although the adverse yaw of the ailerons (negative $C_{n_{\delta_a}}$) and the deterioration of directional stability were discovered early in the program, the pilots continued to have occasional lateral control problems with the FACS off. Figure 19 shows a time history of a sideslip maneuver performed during flight 42 of the XB-70-2 airplane at a Mach number of 0.94 with the wingtips up and the FACS off. During most of the maneuver, the phasing of the aileron and rudder inputs was such that the adverse yaw due to aileron tended to reinforce the yaw due to rudder. The result was a large sideslip excursion.

Dutch-roll characteristics.- A comparison of the flight-determined and predicted Dutch-roll stability characteristics with the FACS off is shown in figure 20 (from ref. 1) for the flight-test conditions listed in table 5. The flight values were calculated from flight-determined derivatives, since nearly all the lateral-directional maneuvers performed in the flight program were of insufficient quality for the direct measurement of Dutch-roll parameters. The calculations were based on the assumption of fixed-rudder conditions. Limited transient oscillation data, however, show that the rudders were actually subject to motion induced by inertial and aerodynamic forces. These forces displaced the rudder actuators, which were arranged so that as one actuator pushed its rudder arm, the other actuator pulled the other rudder. Figure 21 shows a time history of an aileron doublet maneuver in which the rudder motion was induced by the initial rolling acceleration and subsequent sideslip response. As the sideslip motion built up, it became the dominant forcing source of the rudder motion, as evidenced by the in-phase relationship of the sideslip, rudder actuator force, and rudder motion. As a result of this rudder movement, the actual values of Dutch-roll period and damping are slightly lower than those calculated from the flight-determined derivatives without considering the rudder movement.

As shown in figure 20, the flight periods are longer than predicted for all three wingtip configurations. The damping ratios and amplitude ratios are less than predicted for the wingtips up (fig. 20(a)) and at 25° (fig. 20(b)), and higher than predicted for the wingtips full down (fig. 20(c)).

Response to aileron inputs.- The response of an airplane to aileron inputs involves the interaction of the product of inertia, moment of inertia, and aerodynamic stability and control derivatives, and it may be different in direction from that indicated by a nondimensional derivative alone. For the XB-70 airplane, the pilots reported adverse yaw for all flight-test conditions and all configurations, even though $C_{n_{\delta_a}}$ was positive for Mach numbers up to approximately 0.92 in the clean configuration. This difference is due to the second term of the following acceleration parameter:

$$\bar{N}'_{\delta_a} = \left(C_{n_{\delta_a}} + \frac{I_{XZ}}{I_X} C_{l_{\delta_a}} \right) \frac{\bar{q}Sb}{I_Z - \frac{I_{XZ}^2}{I_X}}$$

A complete analysis of an airplane's response characteristics to aileron inputs during closed-loop (pilot/airplane) interactions takes into account oscillatory damping, frequency, roll-to-sideslip ratio, and roll-mode constant. The aileron control dynamic response parameter, $\frac{\omega_\varphi}{\omega_d}$ (refs. 9 and 10), is sensitive to these characteristics. This parameter occurs in the transfer function for $\frac{p}{\delta_a}$ and may be represented to a first order of approximation by the expression

$$\frac{\omega_\varphi}{\omega_d} \approx \left(1 - \frac{\bar{L}'_\beta \bar{N}'_{\delta_a}}{\bar{N}'_\beta \bar{L}'_{\delta_a}} \right)^{1/2}$$

This expression provides qualitative insight into the variations in the response characteristics of lightly damped airplanes like the unaugmented XB-70. Figure 22 shows a nomograph of the above expression and the influence of the acceleration ratios $\frac{\bar{L}'_\beta}{\bar{N}'_\beta}$ and $\frac{\bar{N}'_{\delta_a}}{\bar{L}'_{\delta_a}}$ and the frequency ratio $\frac{\omega_\varphi}{\omega_d}$ on response characteristics.

If the flight data from reference 1 (the same data as used in fig. 20) are applied to figure 22, the yaw response due to aileron inputs proves to be adverse for all configurations throughout the Mach number range of the data. This corresponds with flight observations, even though $C_{n_{\delta_a}}$ is positive for the data points at Mach numbers of 0.61 and 0.79 with the wingtips up. Pilot-induced oscillation tendencies are indicated for all flight Mach numbers with the wingtips at 65° because for these

data the values of $\bar{N}'_{\delta_a}$ are negative and the values of $\bar{L}'_{\beta}$ are positive. These oscillation tendencies were divergent in flight and were more pronounced in the Mach number range from 1.64 to 1.84 than at lower or higher Mach numbers. The data point at $M = 1.20$ for $\delta_T = 25^\circ$ shows lower effective roll control power than at $M = 0.95$ for the same configuration.

Figure 23 shows a flight time history of a roll maneuver at a Mach number of 0.79 which illustrates the strong adverse yaw response to aileron input. With the wingtips deflected 25° and the FACS off, the airplane was subjected to a 6.5° aileron input in order to roll out from a 30° banked turn. Although the static yaw due to aileron and the effective dihedral were both positive, the yaw response to aileron was strongly adverse. Few aileron rolls were performed with the FACS off because of this adverse response in yaw.

The greatest adverse yaw response due to aileron input was encountered at a Mach number of 0.95, where the yaw due to aileron was highly adverse for static conditions and even more so for dynamic conditions. Pilots attempting to perform rollouts from wind-up turns at this Mach number with the FACS off encountered excessive yawing response. The yawing was more severe for the wingtips-up configuration than for the wingtips at 25° because of the large decrease in effective roll control power with the wingtips up (fig. 22).

A divergent pilot-induced oscillation experienced on the XB-70 airplane with the wingtips full down and with the FACS off is illustrated in figure 24. In this instance the pilot deliberately applied aileron to disturb the airplane while flying at Mach 2.51. His subsequent attempts to damp out the disturbance with aileron control inputs resulted in the divergent oscillation. This oscillation was eventually damped out as a result of the airplane's inherent Dutch-roll stability after the pilot released the wheel. With the wingtips full down, the divergent oscillation did not permit the airplane to be maneuvered in roll with the FACS off. Reference 3 includes an illustration of the pilot-induced-oscillation problem under emergency conditions.

Effect of the flight augmentation control system.– From the previous discussion, it is apparent that the FACS was essential during lateral-directional maneuvers with the wingtips full down in order to minimize the divergent pilot-induced-oscillation tendency. The damping due to the FACS was also desirable for the wingtips up and at 25° because of the airplane's light wheel force gradients and its adverse response in yaw due to aileron inputs.

The effectiveness of the FACS in alleviating the airplane's pilot-induced-oscillation tendencies with the wingtips full down is illustrated by the time history in figure 25. This figure shows the pilot-induced oscillation which resulted from the pilot's attempt to recover from a rolloff at a Mach number of 2.5 after a pullup and release maneuver with the FACS off. The divergent oscillations were effectively damped when the FACS was activated. Of interest was the pilot's relative insensitivity to transverse accelerations at the pilot's station, $a_{t_{ps}}$. The lack of lateral motion cues made it necessary for him to refer to the sideslip indicator as an aid in controlling the airplane. Although the divergent oscillation could have been suppressed by releasing the controls without activating the FACS, the airplane would

have returned to the rolloff excursion.

The FACS was deficient in overcoming adverse effects only near a Mach number of 0.95 with the wingtips up. The very high adverse yaw response to aileron inputs and the high effective dihedral with the wingtips up in the vicinity of this Mach number (ref. 1) precluded large aileron inputs even with the FACS on. Rudder power available through the yaw FACS was inadequate to overcome the adverse yawing motion due to aileron inputs of 15°.

Effect of lateral bobweight.- A limited flight assessment of the lateral bobweight was made at a Mach number of approximately 2.5 and an altitude of 18,288 meters (60,000 feet). The flight data that are available show that the device was highly effective as a simple backup system in the event of a failure in the FACS. The effectiveness of the bobweight in suppressing a divergent pilot-induced oscillation during a FACS-off sideslip maneuver performed at a Mach number of 2.51 is illustrated in figure 26. Activation of the lateral bobweight at $t \approx 30$ seconds resulted in the rapid damping of the oscillation and permitted the maneuver to be completed.

CONCLUDING REMARKS

A flight evaluation of the stability and control characteristics of the XB-70 airplane at Mach numbers up to 3.0 and altitudes up to 21,300 meters (70,000 feet) showed the airplane's inherent longitudinal characteristics to be generally satisfactory. In the lateral-directional modes, however, the airplane exhibited troublesome response to aileron inputs.

Differences between the flight-determined and predicted elevator trim settings were largest at high supersonic Mach numbers. At Mach numbers above 1.8, the flight results also showed positive apparent speed stability instead of the predicted negative speed stability. Thus the Mach number trim loop provided in the flight augmentation control system (FACS) to compensate for the predicted negative speed stability was not used.

More pilot concentration was required at high supersonic speeds than at lower speeds in retrimming the airplane following a change in altitude or speed, or both, because of the relative insensitivity of the altimeter and attitude indicator systems. The need for a more sensitive attitude indicator was indicated by the high rate of climb (914 m/min (3000 ft/min)) associated with a 1° change in attitude at a Mach number of 3.0.

Troublesome altitude excursions experienced at Mach numbers above 2.5 in winter were due to regions of varying atmospheric pressure and the pilot's attempts to apply corrective control inputs in response to readings of pressure-sensitive altitude and rate-of-climb instruments.

In the lateral-directional modes, the airplane was characterized by light wheel forces, low static directional stability beyond approximately 2° of sideslip, static adverse yaw due to aileron in the Mach number range from approximately 0.92 to the

maximum tested, adverse yaw response to aileron inputs throughout the entire Mach number range, and negative effective dihedral with the wingtips full down (65°).

With the FACS off, light wheel forces and adverse yaw response to aileron inputs restricted the use of the ailerons. In the supersonic region, with the FACS off, the adverse aileron yaw and negative effective dihedral were conducive to pilot-induced oscillations. These problems were eliminated by using the FACS except when large aileron inputs were made at Mach numbers near 0.95 with the wingtips up.

The lateral bobweight was found to be highly effective as an auxiliary stabilization device in the speed range covered.

Flight Research Center,
National Aeronautics and Space Administration,
Edwards, Calif., Aug. 17, 1973.

REFERENCES

1. Wolowicz, Chester H.; Strutz, Larry W.; Gilyard, Glenn B.; and Matheny, Neil W.: Preliminary Flight Evaluation of the Stability and Control Derivatives and Dynamic Characteristics of the Unaugmented XB-70-1 Airplane Including Comparisons With Predictions. NASA TN D-4578, 1968.

2. Powers, Bruce G.: A Review of Transport Handling-Qualities Criteria in Terms of Preliminary XB-70 Flight Experience. NASA TM X-1584, 1968.

3. Wolowicz, Chester H.: Analysis of an Emergency Deceleration and Descent of the XB-70-1 Airplane Due to Engine Damage Resulting From Structural Failure. NASA TM X-1195, 1966.

4. Mechtly, E. A.: The International System of Units – Physical Constants and Conversion Factors (Revised). NASA SP-7012, 1969.

5. Control Systems Group: Flight Control Systems, XB-70 Air Vehicle. Rep. No. NA-60-2, North American Aviation, Inc., Jan. 4, 1960.

6. Aero-Thermo Design, B-70 Division: Analysis of External Aerodynamic Effect of Inlet Operation on the XB-70 at Mach Numbers of 1.2 to 3.5 in the North American Aviation Trisonic Wind Tunnel and the Ames 8 × 7 Supersonic Wind Tunnel. Rep. No. NA-62-575, North American Aviation, Inc., June 1, 1962.

7. Aerodynamics Group: Estimated Rigid and Flexible Aerodynamic Derivatives for XB-70 Air Vehicle No. 1. Rep. No. TFD-65-396, North American Aviation, Inc., June 21, 1965 (rev. Oct. 6, 1966).

8. Wykes, John H.; and Lawrence, Robert E.: Estimated Performance and Stability and Control Data for Correlation With XB-70-1 Flight Test Data. NASA CR-114335, 1971.

9. Newell, F. D.: Criteria for Acceptable Representation of Airplane Dynamic Responses in Simulators Used for Pilot Training. NAVTRADEVCEN 1146-1 (Contract No. N61339-1146), Cornell Aero. Lab., Oct. 1962.

10. Wolowicz, Chester H.; and Yancey, Roxanah B.: Lateral-Directional Aerodynamic Characteristics of Light, Twin-Engine, Propeller-Driven Airplanes. NASA TN D-6946, 1972.

TABLE 1.– GEOMETRIC CHARACTERISTICS OF THE XB-70-1 AIRPLANE

Wing –	
Total area, includes 230.62 m^2 (2482.34 ft^2) covered by fuselage but not 3.12 m^2 (33.53 ft^2) of the wing ramp area, m^2 (ft^2)	585.07 (6297.8)
Span, m (ft)	32 (105)
Aspect ratio	1.751
Taper ratio	0.019
Dihedral angle, deg	0
Root chord (wing station 0), m (ft)	35.89 (117.76)
Tip chord (wing station 16 m (630 in.)), m (ft)	0.67 (2.19)
Mean aerodynamic chord, m (in.):	23.94 (942.38)
Wing station, m (in.)	5.43 (213.85)
Fuselage station of 25-percent wing mean aerodynamic chord, m (in.)	41.18 (1621.22)
Sweepback angle, deg:	
Leading edge	65.57
25-percent element	58.79
Trailing edge	0
Airfoil section	0.30 to 0.70 HEX (MOD)
Thickness, percent chord:	
Wing station –	
Root to 4.72 m (186 in.)	2.0
11.68 m to 16 m (460 in. to 630 in.)	2.5
Folding wingtip (data for one tip only) –	
Area, m^2 (ft^2)	48.39 (520.90)
Span, m (ft)	6.33 (20.78)
Aspect ratio	0.829
Taper ratio	0.046
Root chord (wing station 9.67 m (380.62 in.)), m (ft)	14.61 (47.94)
Tip chord (wing station 16 m (630 in.)), m (ft)	0.67 (2.19)
Mean aerodynamic chord (wing station 11.87 m (467.37 in.)), m (in.)	9.76 (384.25)
Down deflection from inboard wing, deg	0, 25, 65
Elevons (data for one side) –	
Total effective area aft of hinge line, includes 0.31 m^2 (3.33 ft^2) air gap at wingtip fold line, m^2 (ft^2)	18.37 (197.7)
Span, m (ft):	
Wingtips up	6.23 (20.44)
Wingtips down	4.26 (13.98)
Chord, m (in.)	2.95 (116)
Sweepback of hinge line, deg	0
Canard –	
Area, includes 13.96 m^2 (150.31 ft^2) covered by fuselage, m^2 (ft^2)	38.61 (415.59)
Span, m (ft)	8.78 (28.81)
Aspect ratio	1.997
Taper ratio	0.388
Dihedral angle, deg	0
Root chord (canard station 0), m (ft)	6.34 (20.79)
Tip chord (canard station 4.39 m (172.86 in.)), m (ft)	2.46 (8.06)
Mean aerodynamic chord, m (in.):	4.68 (184.3)
Canard station, m (in.)	1.87 (73.71)
Fuselage station of 25-percent canard mean aerodynamic chord, m (in.)	14.06 (553.73)
Sweepback angle, deg:	
Leading edge	31.70
25-percent element	21.64
Trailing edge	-14.91
Airfoil section	0.34 to 0.66 HEX (MOD)
Thickness chord ratio, percent:	
Root	2.5
Tip	2.52
Ratio of canard area to wing area	0.066

TABLE 1.- GEOMETRIC CHARACTERISTICS OF THE XB-70-1 AIRPLANE - Concluded

Canard flap (data for one side) -	
Area (aft of hinge line), m^2 (ft^2)	5.08 (54.69)
Inboard chord (canard station 1.22 m (47.93 in.)), m (ft)	2.18 (7.16)
Outboard chord (canard station 4.39 m (172.86 in.)), m (ft)	1.02 (3.34)
Ratio of flap area to canard semiarea	0.263
Vertical tail (one of two) -	
Area (includes 0.83 m^2 (8.96 ft^2) blanketed area), m^2 (ft^2)	21.74 (233.96)
Span, m (ft)	4.57 (15)
Aspect ratio	1
Root chord (vertical-tail station 0), m (ft)	7.03 (23.08)
Tip chord (vertical-tail station 4.57 m (180 in.)), m (ft)	2.11 (6.92)
Taper ratio	0.30
Mean aerodynamic chord, m (in.):	5.01 (197.40)
Vertical-tail station, m (in.)	1.88 (73.85)
Fuselage station of 25-percent vertical-tail mean aerodynamic chord	55.59 (2188.50)
Sweepback angle, deg:	
Leading edge	51.77
25-percent element	45
Trailing edge	10.89
Airfoil section	0.30 to 0.70 HEX (MOD)
Thickness chord ratio, percent:	
Root	3.75
Tip	2.50
Cant angle, deg	0
Ratio of vertical-tail area to wing area	0.037
Rudder -	
Area, includes 0.81 m^2 (8.66 ft^2) blanketed area, m^2 (ft^2)	17.76 (191.11)
Span, m (ft)	4.57 (15.00)
Root chord (vertical-tail station 0), m (ft)	2.79 (9.16)
Tip chord (vertical-tail station 4.57 m (180 in.)), m (ft)	2.11 (6.92)
Sweepback of hinge line	-45.0
Ratio of rudder area to vertical-tail area	0.82
Fuselage (includes canopy) -	
Length, m (ft)	56.62 (185.75)
Maximum depth (fuselage station 22.30 m (878 in.)), m (in.)	2.72 (106.92)
Maximum breadth (fuselage station 21,72 m (855 in.)), m (in.)	2.54 (100)
Side area, m^2 (ft^2)	87.30 (939.72)
Planform area, m^2 (ft^2)	110.07 (1184.78)

TABLE 2.- TRAVEL LIMITS AND MAXIMUM RATES OF TRAVEL OF COCKPIT CONTROLS AND CONTROL SURFACES

(a) Cockpit controls

Column -	
Travel limit, cm (in.)	-9.15 (-3.6), 13.83 (5.45)
Free play, cm (in.)	0.254 (0.10)
Breakout force, N (lb)	22.2 (5.16)
Wheel -	
Travel limit, deg	81
Free play, deg	1.8
Breakout force, N (lb)	13.3 (3)
Pedal (adjustable) -	
Travel limit, cm (in.)	±8.9 (±3.5) to ±10.2 (±4.0)
Free play, cm (in.)	0.127 (0.05)
Breakout force, N (lb)	62.3 (14)

(b) Control surfaces

Elevon -	
Maximum trailing-edge-up travel, deg:	
Pitch	25
Roll	15
Total	30
Maximum trailing-edge-down travel, deg:	
Pitch	15
Roll	15
Total	30
Maximum rate of travel, deg/sec:	
Pitch	28
Roll, per surface	28
Total	56
Rudder -	
Maximum travel, deg:	
Landing gear down	±12
Landing gear up	±3
Maximum rate of travel, deg/sec	12
Canard -	
Maximum travel, deg	0 to 6 (leading edge up)
Maximum rate of travel, deg/sec	4.2
Flap -	
Maximum travel (two positions only), deg	0, 20 (trailing edge down)

TABLE 3.– XB-70 INSTRUMENTATION PERTINENT TO STABILITY AND CONTROL

Parameter	Accuracy, percent of full range	Transducer range	Sampling rate, per sec
Central air-data system altitude (coarse)	2.0	-305 to 30,480 m (-1,000 to 100,000 ft)	4
Central air-data system altitude (fine)	1.0	152.4 m/rev (5,000 ft/rev)	40
Central air-data system Mach number (coarse)	2.0	0.5 to 3.2	4
Central air-data system Mach number (fine)	2.0	0.3 M/rev	40
Angle of attack	0.8	-10° to 30°	20
Angle of sideslip	0.8	±20°	20
Pitch attitude	2.0	-10° to 40°	20
Bank attitude	2.0	±45°	20
Pitch rate	2.0	±10 deg/sec	[c]4
Roll rate	2.0	±100 deg/sec	[c]4
Yaw rate	2.0	±10 deg/sec	[c]4
Pitch acceleration[a]	2.0	±0.5 rad/sec/sec	20
Roll acceleration[a]	2.0	±1.0 rad/sec/sec	20
Yaw acceleration[b]	2.0	±0.5 rad/sec/sec	20
Normal acceleration	2.0	±2g	20
Transverse acceleration	2.0	±1g	20
Left-hand wingtip position	2.0	0° to 65°	4
Right-hand wingtip position	2.0	0° to 65°	4
Left-hand canard position	2.0	0° to 6°	20
Left-hand vertical-stabilizer position	1.0	±12°	20
Right-hand vertical-stabilizer position	1.0	±12°	20
Position of individual elevon segment	1.2	±30°	20

[a]Pitch and roll accelerometers installed after flight 52.

[b]Yaw accelerometer installed after flight 59.

[c]Sample rate changed to 20 samples/sec after flight 49.

TABLE 4.- XB-70-1 FLIGHT CONDITIONS FOR LONGITUDINAL DATA

[From ref. 1]

δ_T, deg	M	h_p, m (ft)		W, N (lb)		Center of gravity, percent $\bar{c}$	α_{trim}, deg	$\delta_{e_{trim}}$, deg	I_Y, kg-m^2 (slug-ft^2)	
[a]0	0.49	3.11×10^3	(10.2×10^3)	1.770×10^6	(0.398×10^6)	21.1	7.0	10.3	28.0×10^6	(20.7×10^6)
[a]0	0.49	3.11	(10.2)	1.766	(0.397)	21.2	6.8	10.2	27.9	(20.6)
0	0.60	3.38	(11.1)	1.890	(0.425)	21.9	6.3	3.3	28.6	(21.1)
0	0.61	5.79	(19.0)	1.908	(0.429)	21.9	8.2	0.2	28.7	(21.2)
0	0.79	7.62	(25.0)	1.690	(0.380)	21.8	5.5	2.8	26.0	(19.2)
0	1.03	10.39	(34.1)	1.592	(0.358)	22.6	4.2	6.8	23.4	(17.3)
0	1.11	10.76	(35.3)	1.526	(0.343)	23.1	4.2	8.0	23.0	(17.0)
25	0.80	3.17	(10.4)	2.113	(0.475)	21.8	4.4	8.0	29.2	(21.6)
25	0.80	3.29	(10.8)	2.108	(0.474)	21.7	4.2	8.0	29.2	(21.6)
25	0.95	7.62	(25.0)	1.566	(0.352)	20.8	3.6	4.6	24.6	(18.2)
25	0.95	10.79	(35.4)	1.704	(0.383)	21.1	5.8	2.0	23.4	(17.3)
25	1.20	12.65	(41.5)	1.383	(0.311)	21.4	5.1	4.8	22.9	(16.9)
25	1.40	12.44	(40.8)	1.606	(0.361)	19.7	4.4	4.8	23.7	(17.5)
25	1.40	12.56	(41.2)	1.601	(0.360)	19.7	4.2	5.2	23.7	(17.5)
65	1.61	13.72	(45.0)	1.641	(0.369)	19.8	3.6	5.9	25.3	(18.7)
65	1.79	16.52	(54.2)	1.388	(0.312)	22.0	4.5	6.0	22.8	(16.8)
65	1.81	13.72	(45.0)	1.779	(0.400)	21.6	3.5	6.1	28.4	(21.0)
65	2.11	16.70	(54.8)	1.619	(0.364)	20.7	4.0	3.1	26.7	(19.7)
65	2.12	15.24	(50.0)	1.739	(0.391)	21.2	4.0	5.9	27.4	(20.2)
65	2.24	17.56	(57.6)	1.526	(0.343)	20.0	4.7	-1.1	25.7	(19.0)
65	2.33	16.67	(54.7)	1.837	(0.413)	20.8	4.4	3.3	28.4	(21.0)
65	2.51	18.35	(60.2)	1.695	(0.381)	21.9	4.1	5.7	27.1	(20.2)
65	2.56	19.72	(64.7)	1.472	(0.331)	23.9	5.0	6.9	23.0	(17.1)

[a]Gear and flaps down.

TABLE 5.- XB-70-1 FLIGHT CONDITIONS FOR LATERAL-DIRECTIONAL DATA

[From ref. 1]

δ_T, deg	M	h_p, m (ft)	W, N (lb)	Center of gravity, $\frac{}{c}$ percent	α_{trim}, deg	$\delta_{e_{trim}}$, deg	I_X, kg-m^2 (slug-ft^2)	I_Z, kg-m^2 (slug-ft^2)	I_{XZ}, kg-m^2 (slug-ft^2)
[a]0	0.51	4.69×10^3 (15.4×10^3)	1.419×10^6 (0.319×10^6)	22.1	5.5	10.4	2.03×10^6 (1.50×10^6)	24.2×10^6 (17.9×10^6)	-0.84×10^6 (-0.620×10^6)
0	0.61	6.04 (19.8)	1.971 (0.443)	19.8	8.6	0	2.92 (2.16)	31.6 (23.3)	-1.260 (-0.930)
0	0.79	7.62 (25.0)	1.681 (0.378)	21.8	5.2	2.5	2.68 (1.98)	29.8 (22.0)	-1.060 (-0.780)
0	0.95	10.67 (35.0)	1.690 (0.380)	22.5	4.8	1.1	1.97 (1.46)	25.2 (18.6)	-1.050 (-0.775)
25	0.80	3.08 (10.1)	1.343 (0.302)	23.2	1.9	6.2	1.82 (1.34)	22.8 (16.8)	-0.798 (-0.590)
25	0.95	7.83 (25.7)	1.548 (0.348)	20.3	3.7	4.5	2.12 (1.57)	26.7 (19.8)	-0.980 (-0.730)
25	1.20	12.19 (40.0)	1.748 (0.393)	20.0	4.3	3.8	2.53 (1.95)	30.2 (22.3)	-1.150 (-0.850)
65	1.41	12.89 (42.3)	1.677 (0.377)	19.7	4.2	7.1	2.25 (1.66)	27.5 (20.4)	-1.060 (-0.781)
65	1.64	13.56 (44.5)	1.624 (0.365)	20.5	3.3	6.8	2.25 (1.66)	27.2 (20.1)	-1.010 (-0.743)
65	1.84	15.06 (49.4)	1.557 (0.350)	21.1	3.4	3.7	2.06 (1.52)	24.7 (18.2)	-1.010 (-0.748)
65	2.10	14.97 (49.1)	1.704 (0.383)	20.3	4.2	4.9	2.48 (1.83)	29.0 (21.4)	-1.080 (-0.800)
65	2.35	16.92 (55.5)	1.735 (0.390)	21.9	4.4	4.7	2.54 (1.88)	30.2 (22.4)	-1.190 (-0.881)

[a]Gear and flaps down.

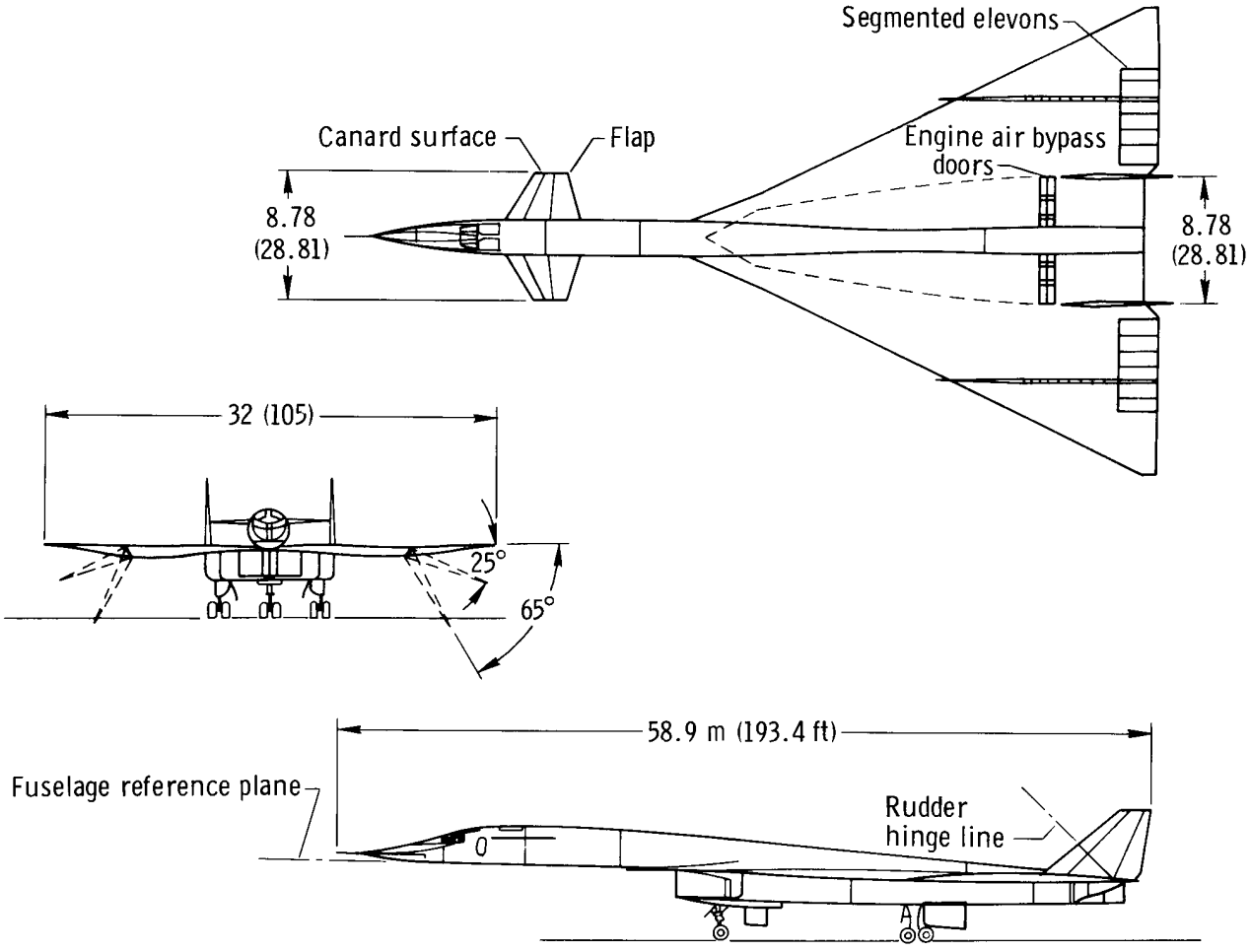

Figure 1. XB-70-1 airplane. Dimensions are in meters (feet) except where otherwise indicated.

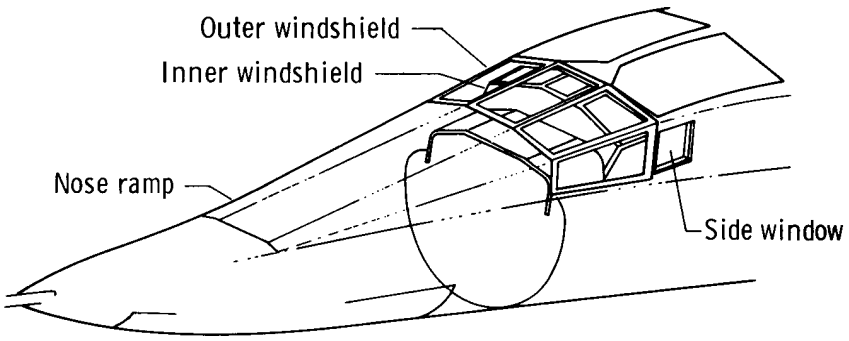

(a) Windshield arrangement.

(b) Nose ramp down.

(c) Nose ramp up.

Figure 2. XB-70 windshield.

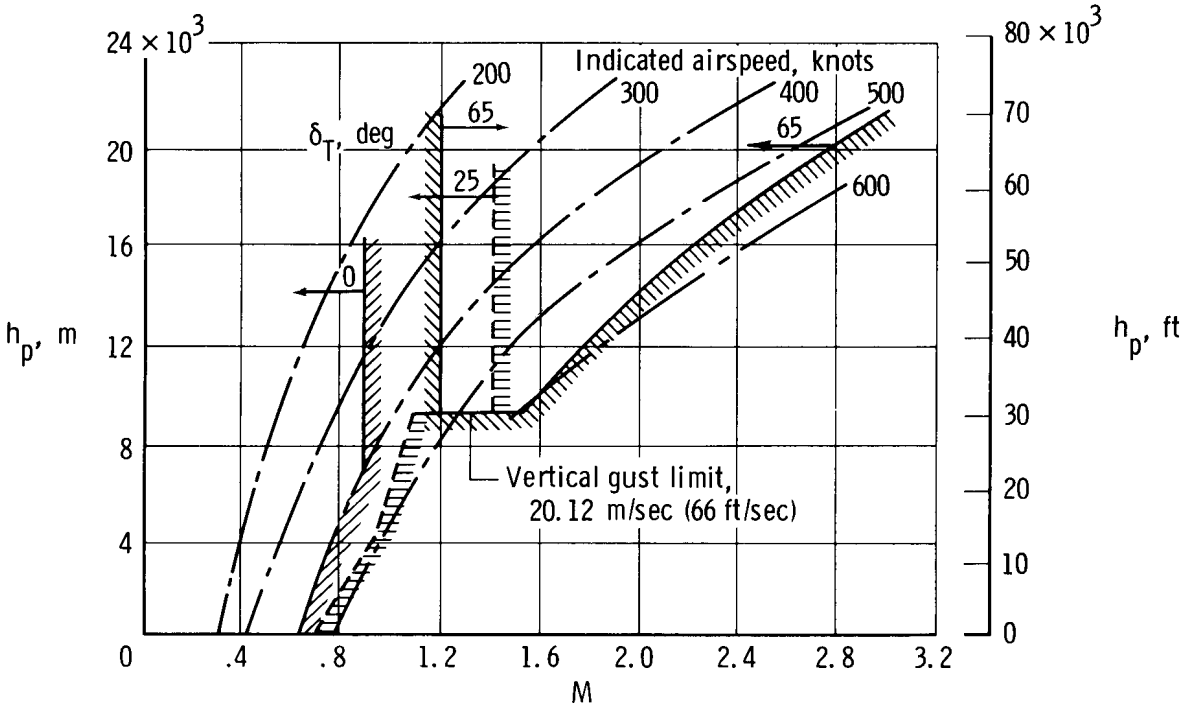

Figure 3. Operational limits of the three wingtip configurations of the XB-70 aircraft.

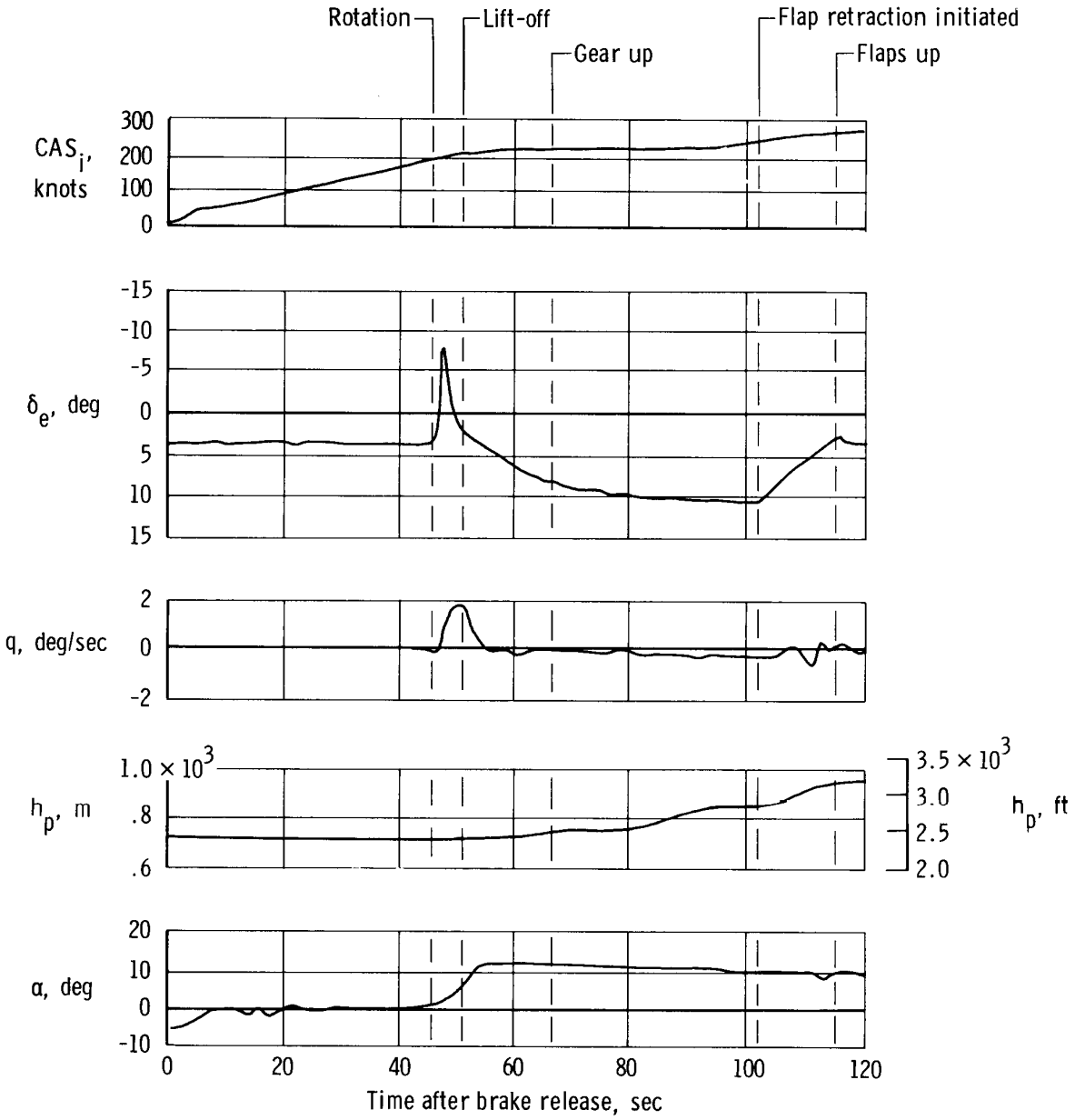

Figure 4. Typical takeoff time history. FACS on; W = 2,397,600 N (539,000 lb); center of gravity = 0.225$\bar{c}$.

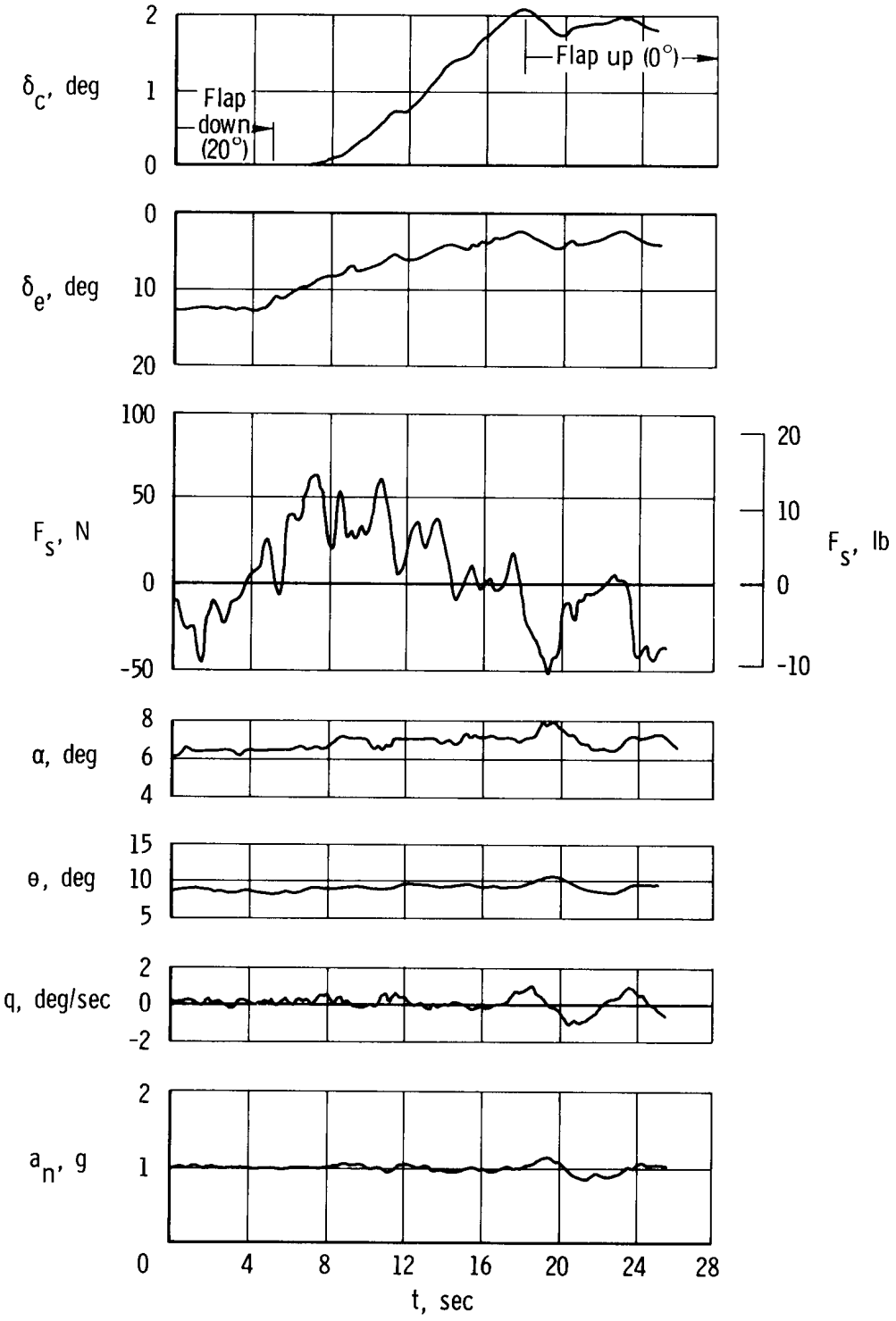

Figure 5. Time history of a typical canard flap retraction. FACS off; M = 0.47; h_p = 2150 m (7000 ft); W = 1,810,400 N (407,000 lb); center of gravity = 0.233$\bar{c}$.

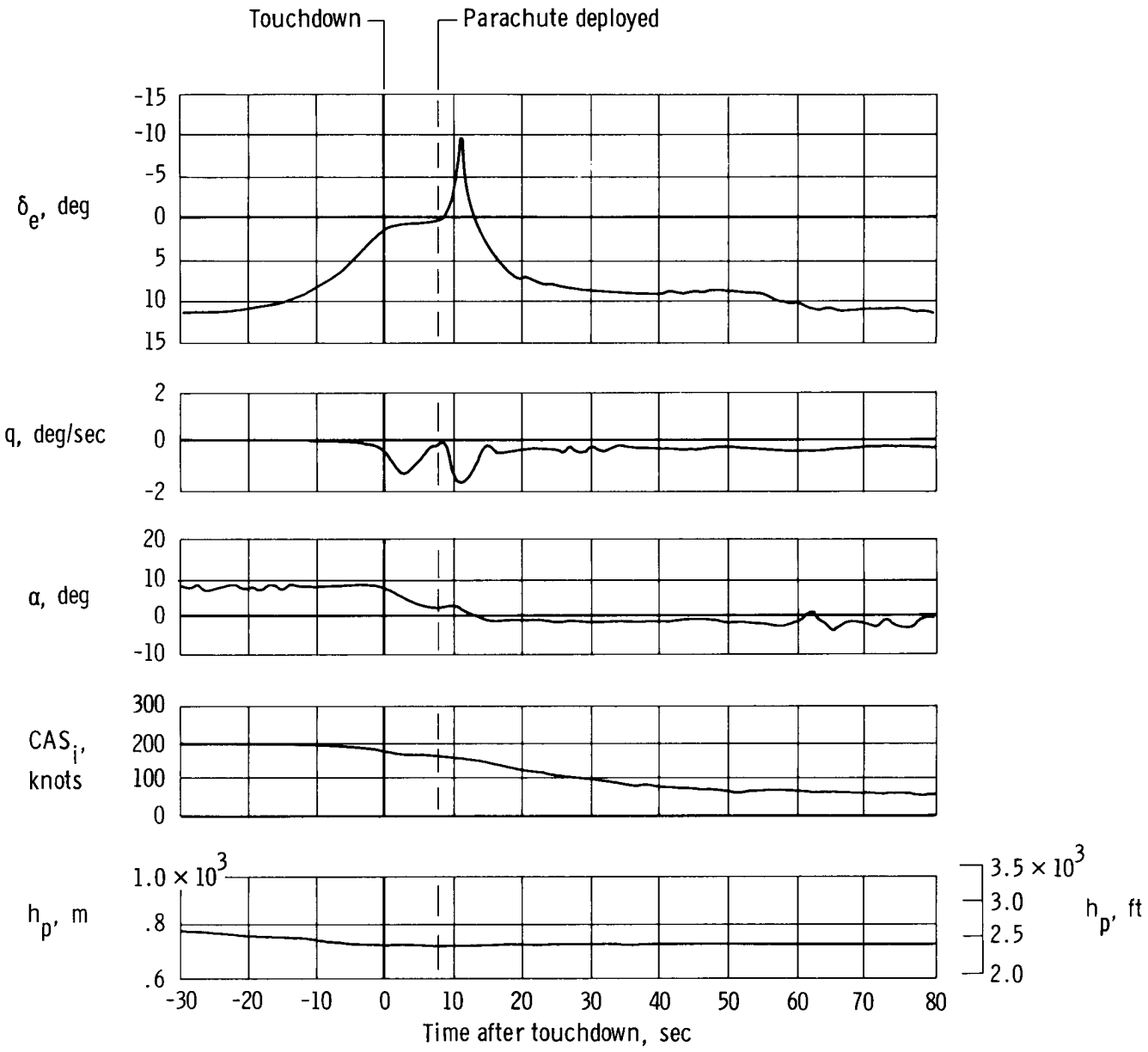

Figure 6. Typical landing time history with flaps down. FACS off; W = 1,298,900 N (292,000 lb); center of gravity = 0.239$\bar{c}$.

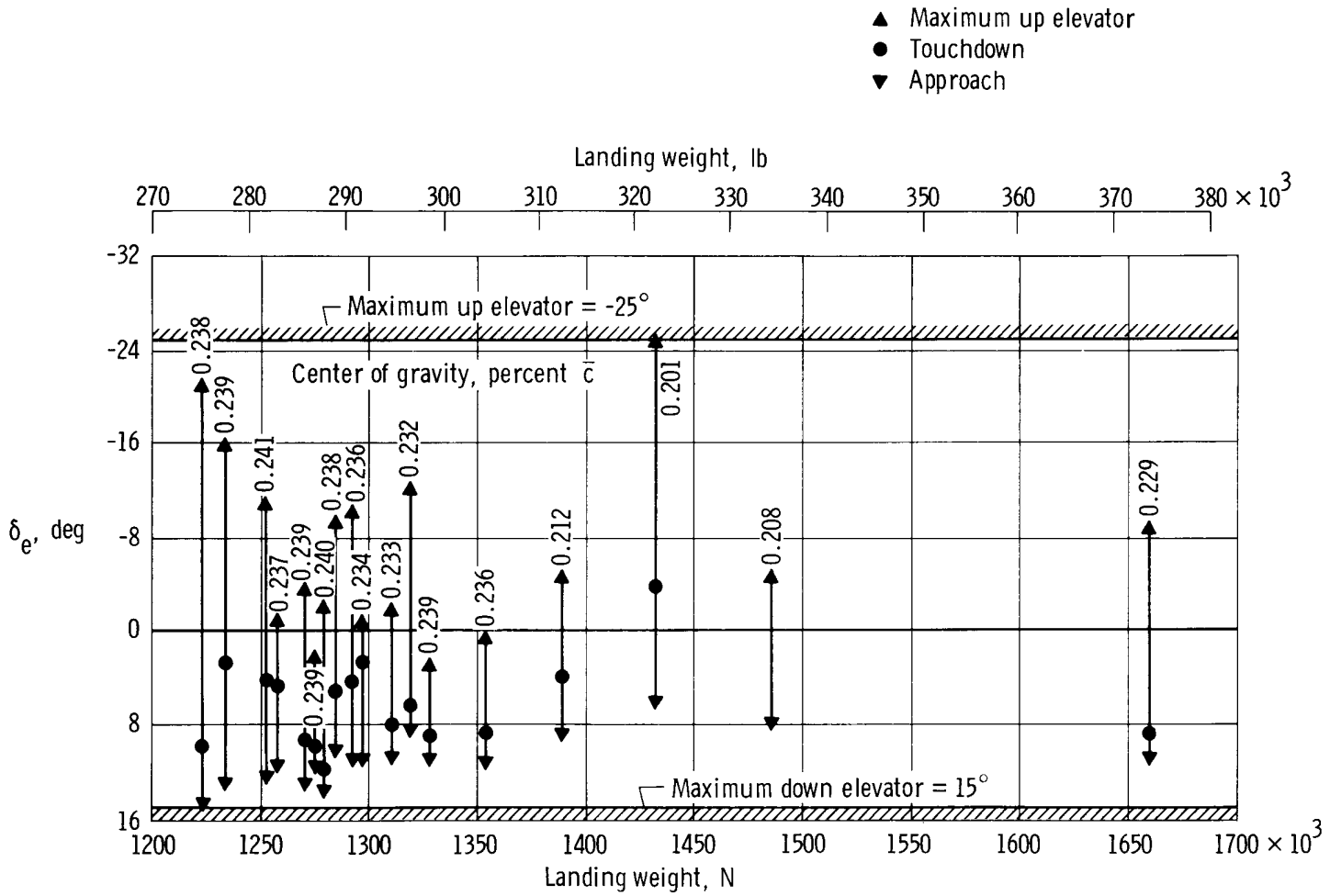

Figure 7. Bar graph of range of elevator deflection on landing. Flaps down.

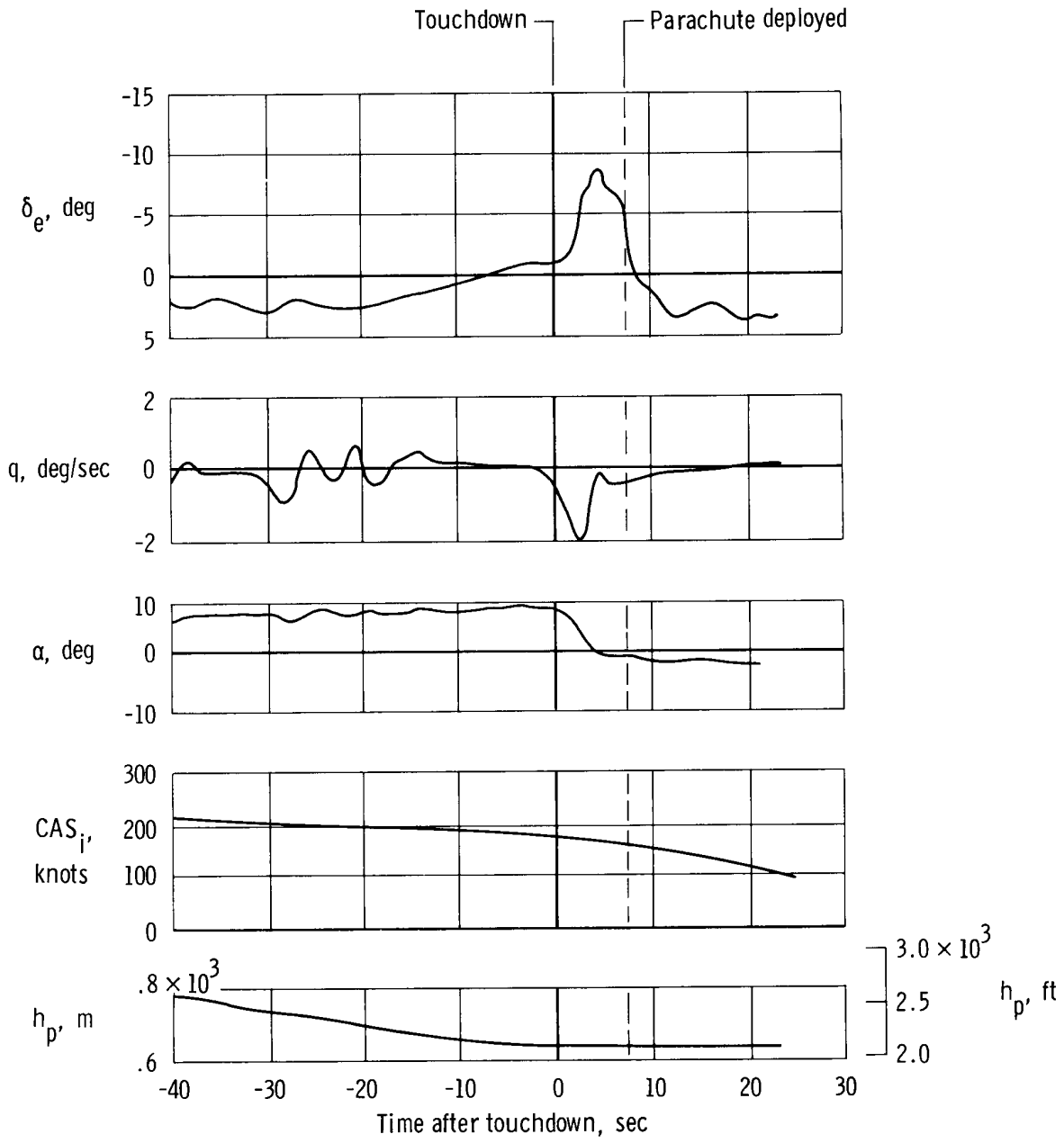

Figure 8. Typical landing time history with flaps up. FACS off; W = 1,298,900 N (292,000 lb); center of gravity = 0.238$\bar{c}$.

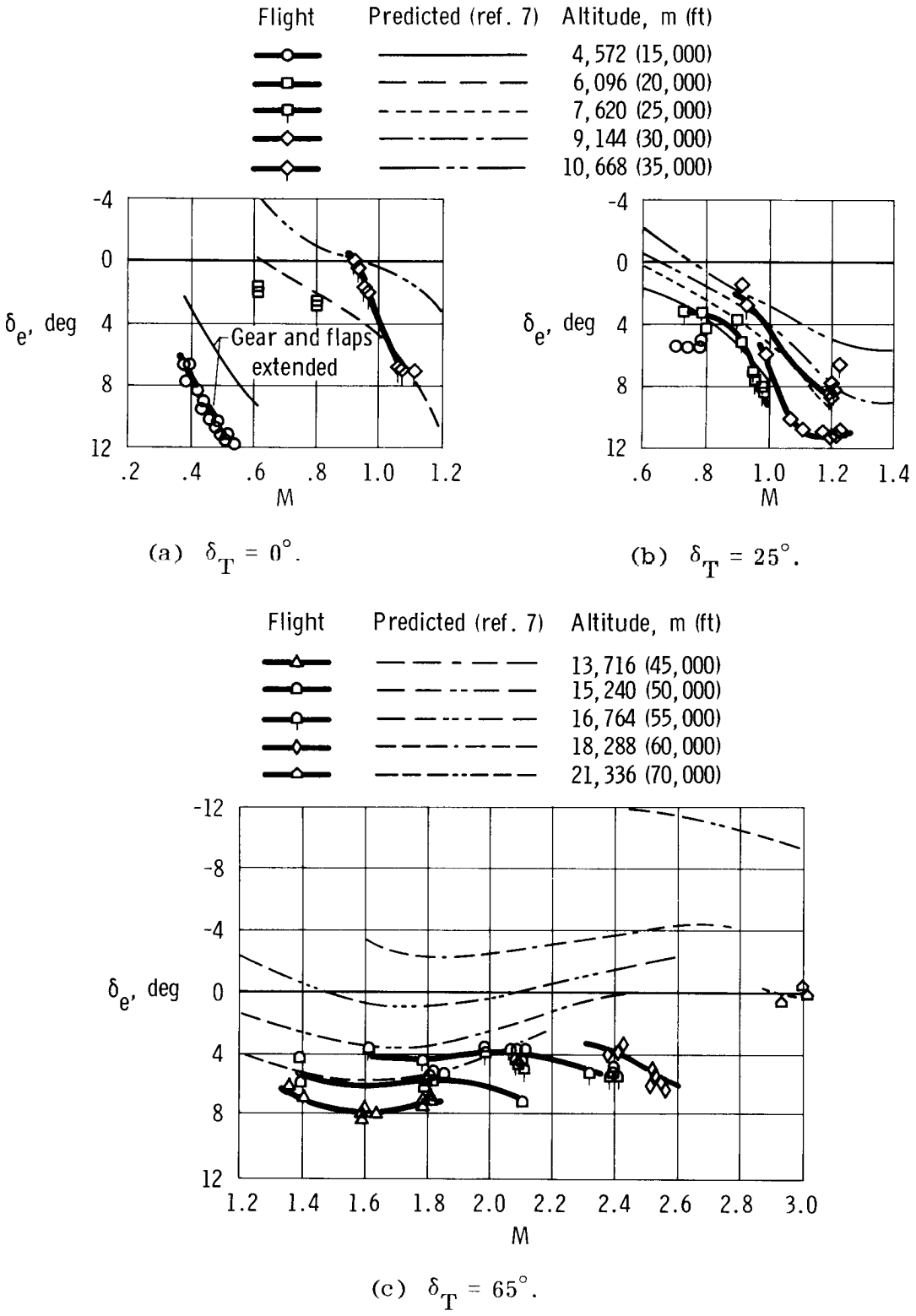

Figure 9. Comparison of flight-determined and predicted longitudinal trim at normalized weight of 1,645,800 N (370,000 lb) and $0.222\bar{c}$ center-of-gravity condition.

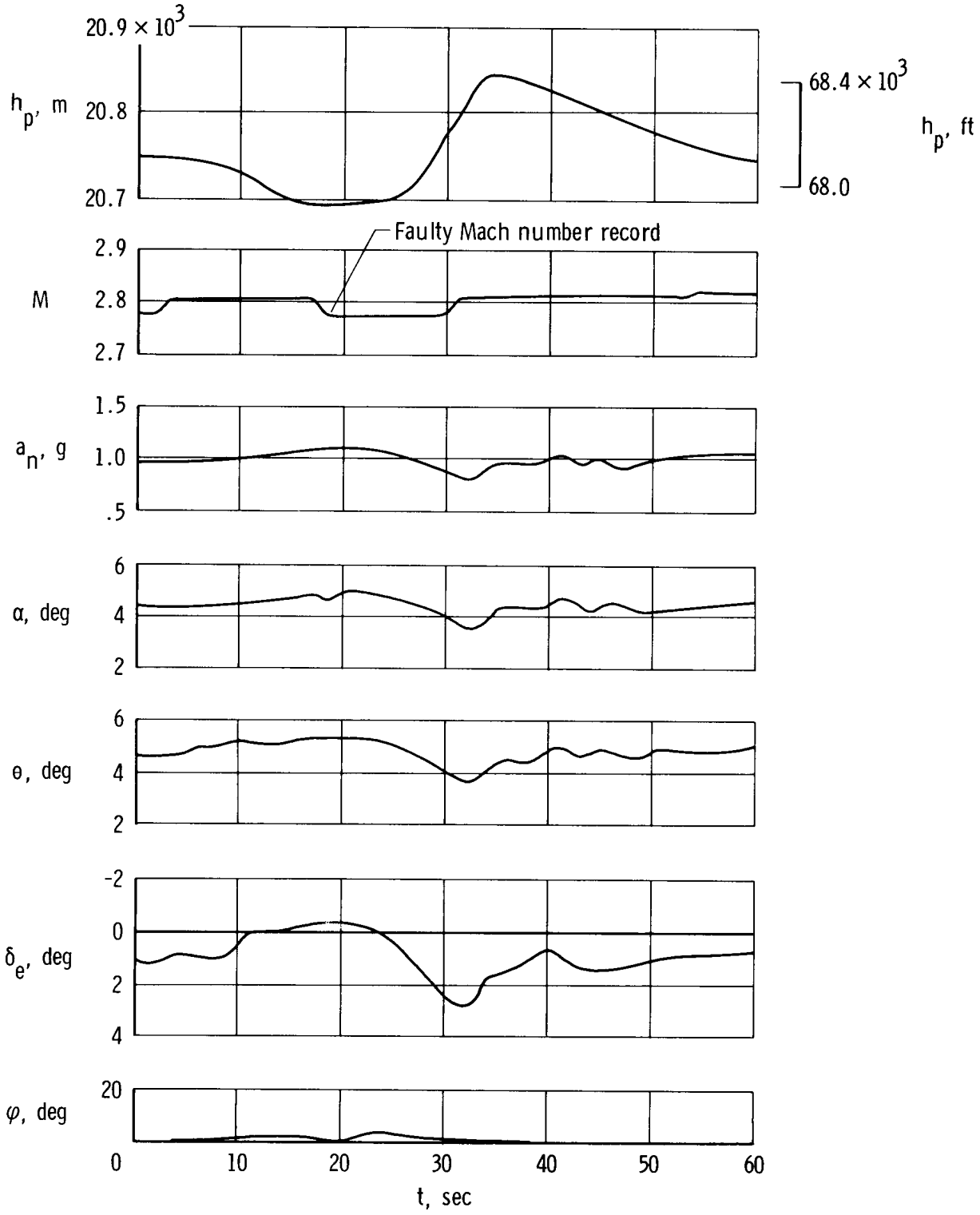

Figure 10. Time history of atmospherically induced longitudinal trim excursions of the XB-70-2 airplane with the pilot in the loop. W = 1,530,600 N (344,100 lb); center of gravity = 0.231$\bar{c}$.

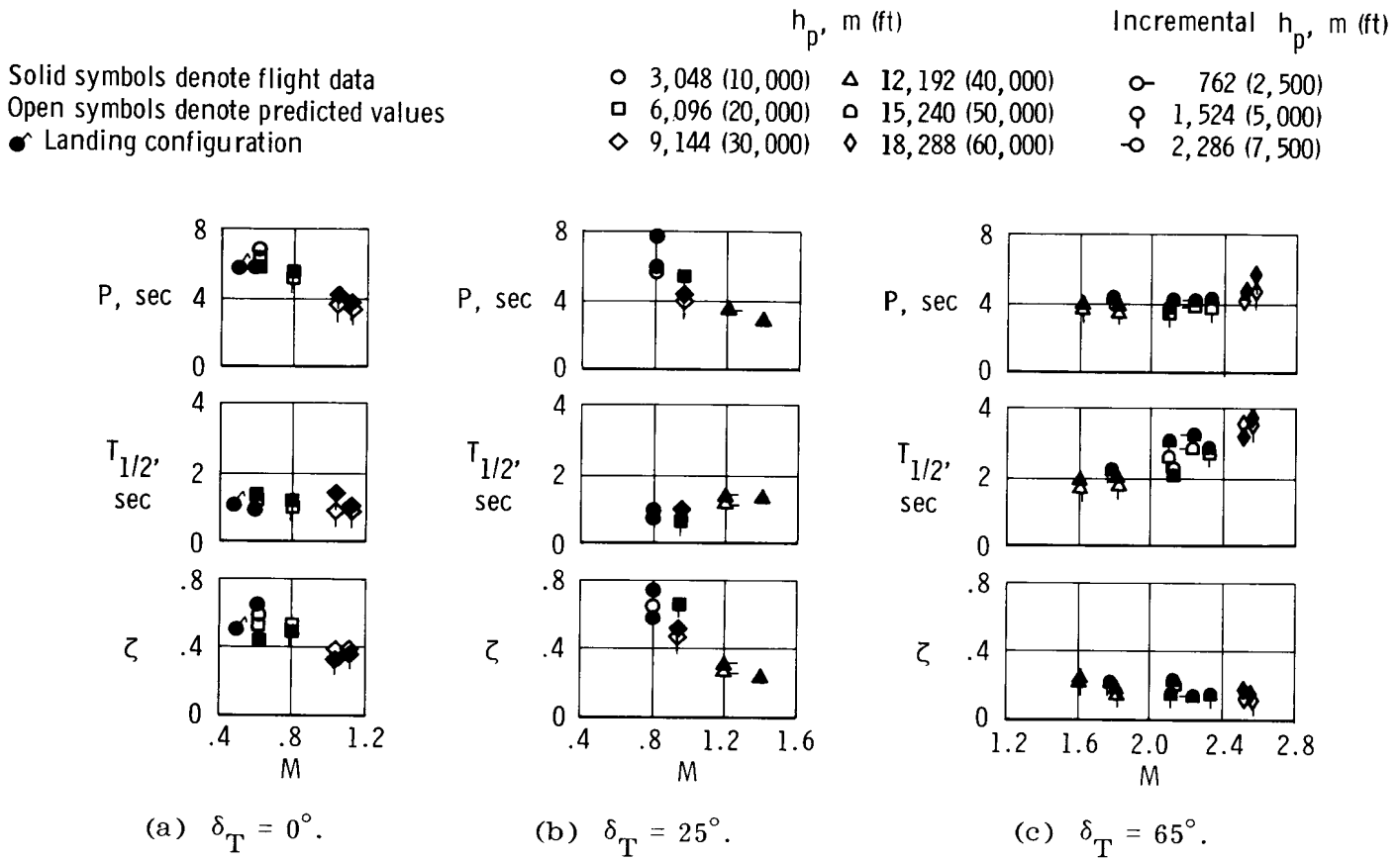

Figure 11. Comparison of flight-determined and predicted longitudinal short-period and damping characteristics (from ref. 1). Weight and center of gravity for individual data points listed in table 4.

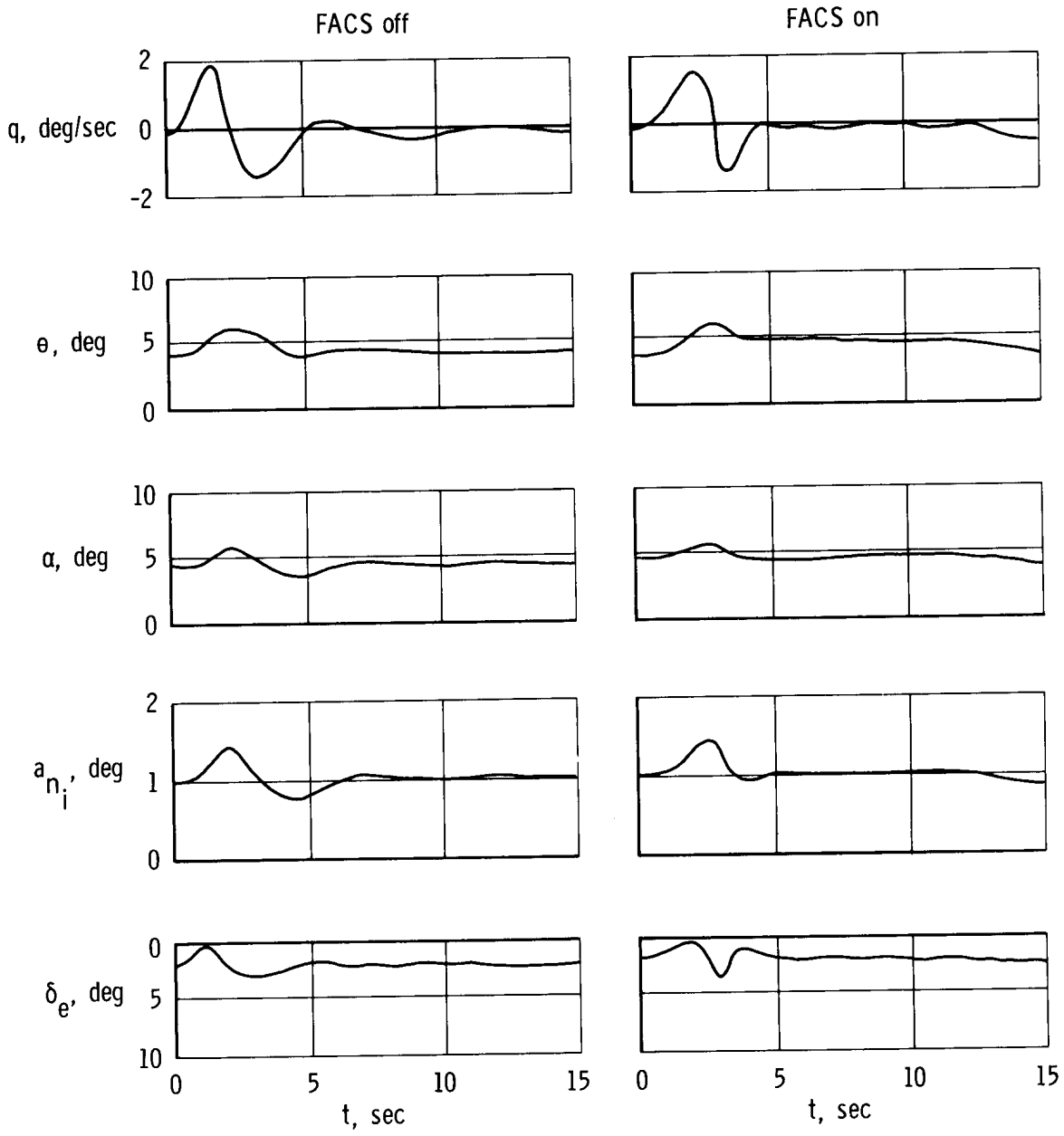

(a) $\delta_T = 25°$, M = 0.80, h_p = 7630 m (25,000 ft).

Figure 12. Effect of pitch FACS on the damping of longitudinal motions.

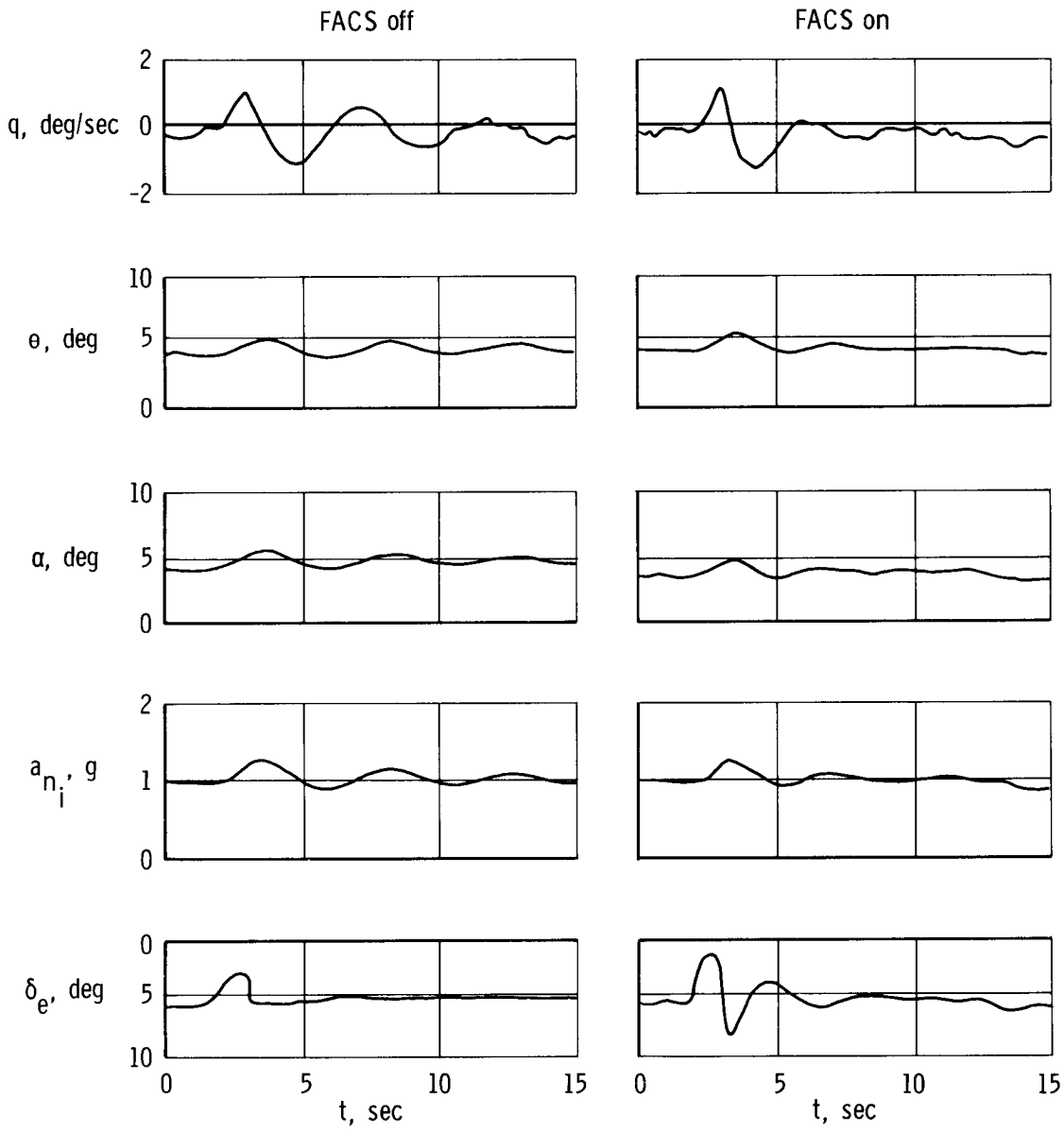

(b) $\delta_T = 65°$, M = 2.50, h_p = 18,300 m (60,000 ft).

Figure 12. Concluded.

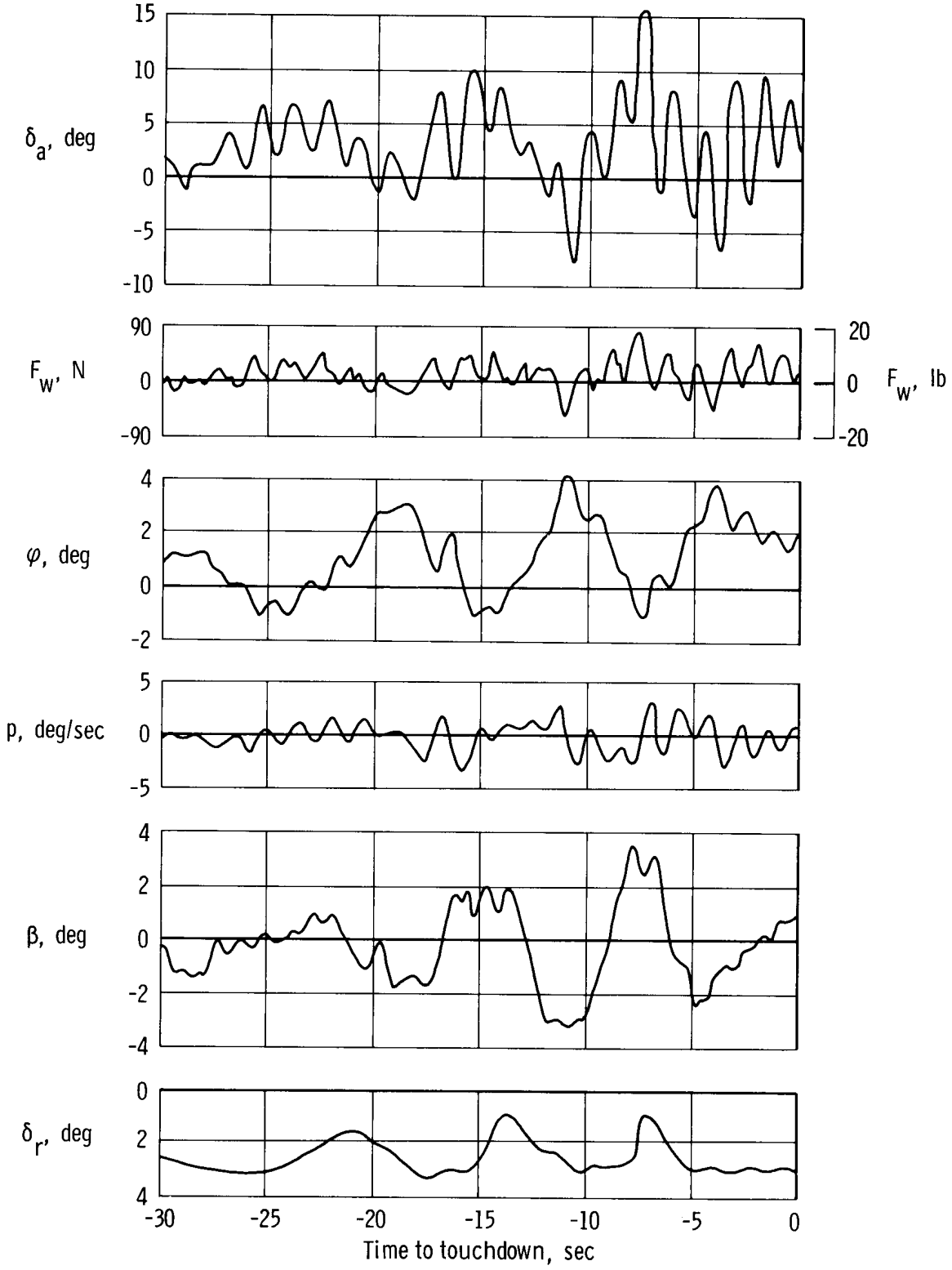

Figure 13. Time history of typical lateral-directional control during landing approach at the beginning of the flight-test program. FACS: yaw off, pitch and roll on; W = 1,325,600 N (298,000 lb); center of gravity = 0.234$\bar{c}$; touchdown velocity = 175 knots.

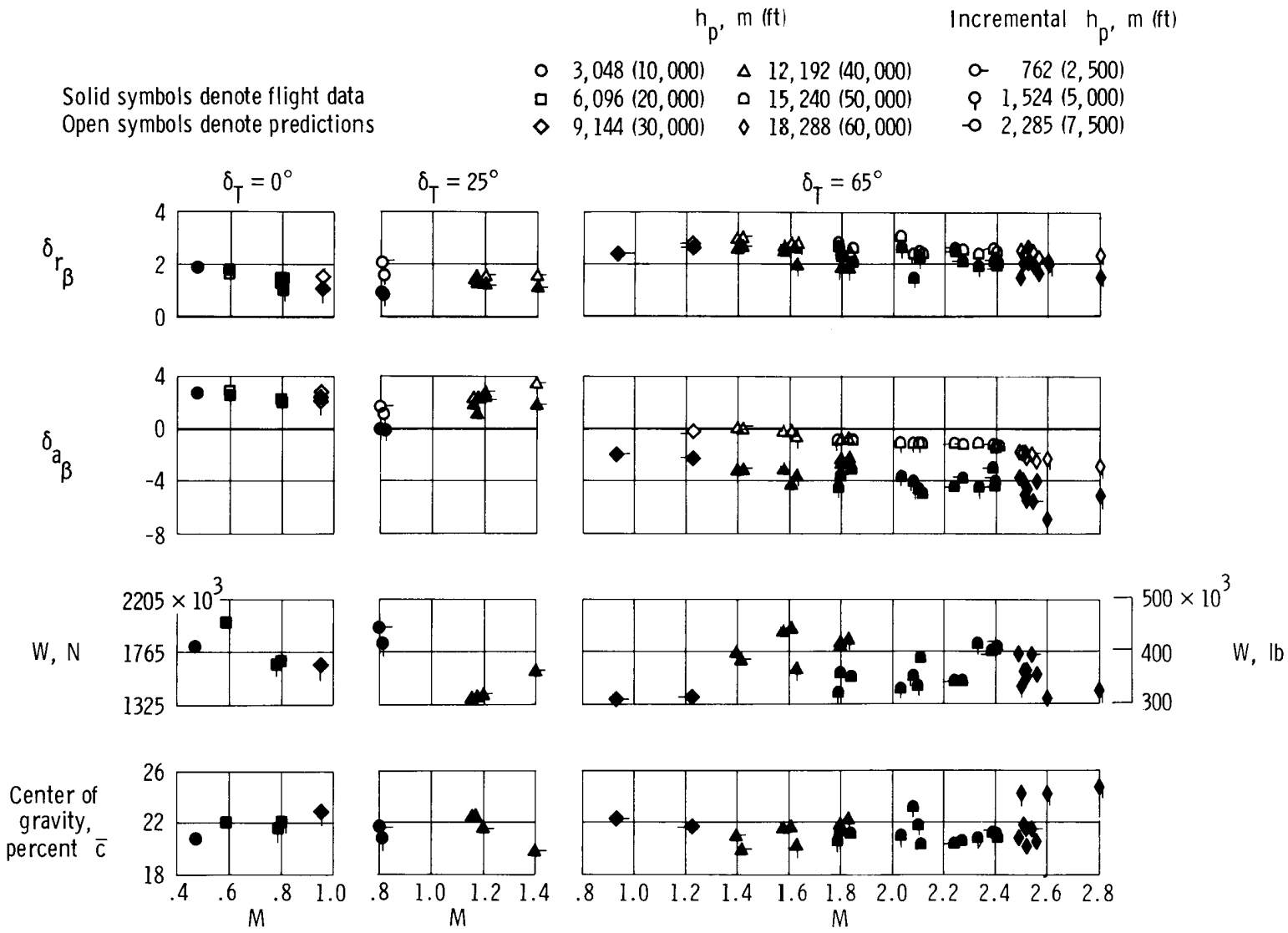

Figure 14. Comparison of flight-determined apparent directional stability and effective dihedral derivatives with predictions at flight-test conditions.

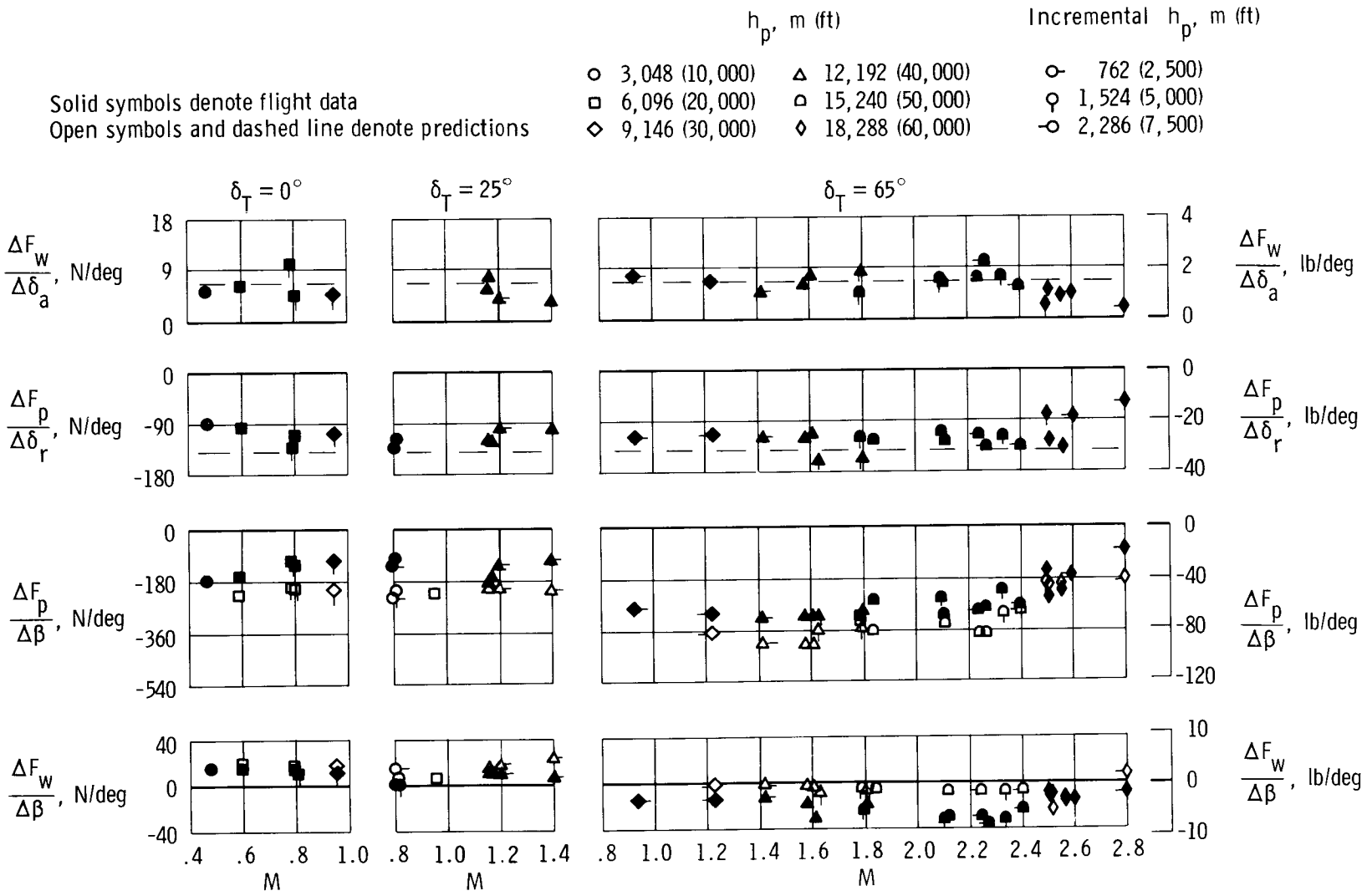

Figure 15. Comparison of flight-determined pedal and wheel force gradients with predictions at flight-test conditions.

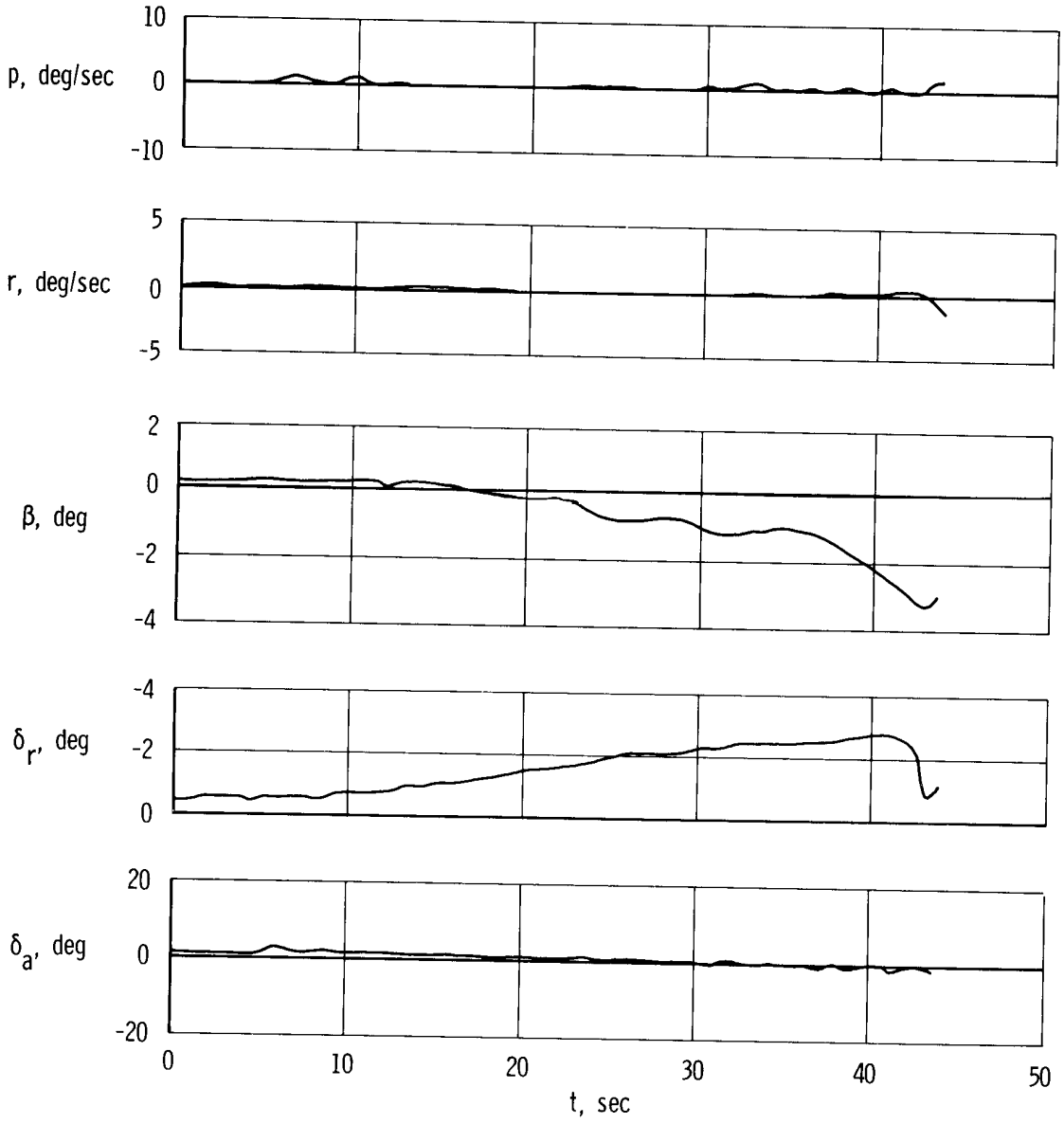

(a) Time history of sideslip maneuver.

Figure 16. Flight data with FACS on showing decrease in static directional stability at $\beta \approx 1.5^{\circ}$. M = 1.20; h_p = 10,400 m (34,100 ft); W = 1,414,530 N (318,000 lb); center of gravity = $0.225\bar{c}$; $\delta_e = 10.9^{\circ}$.

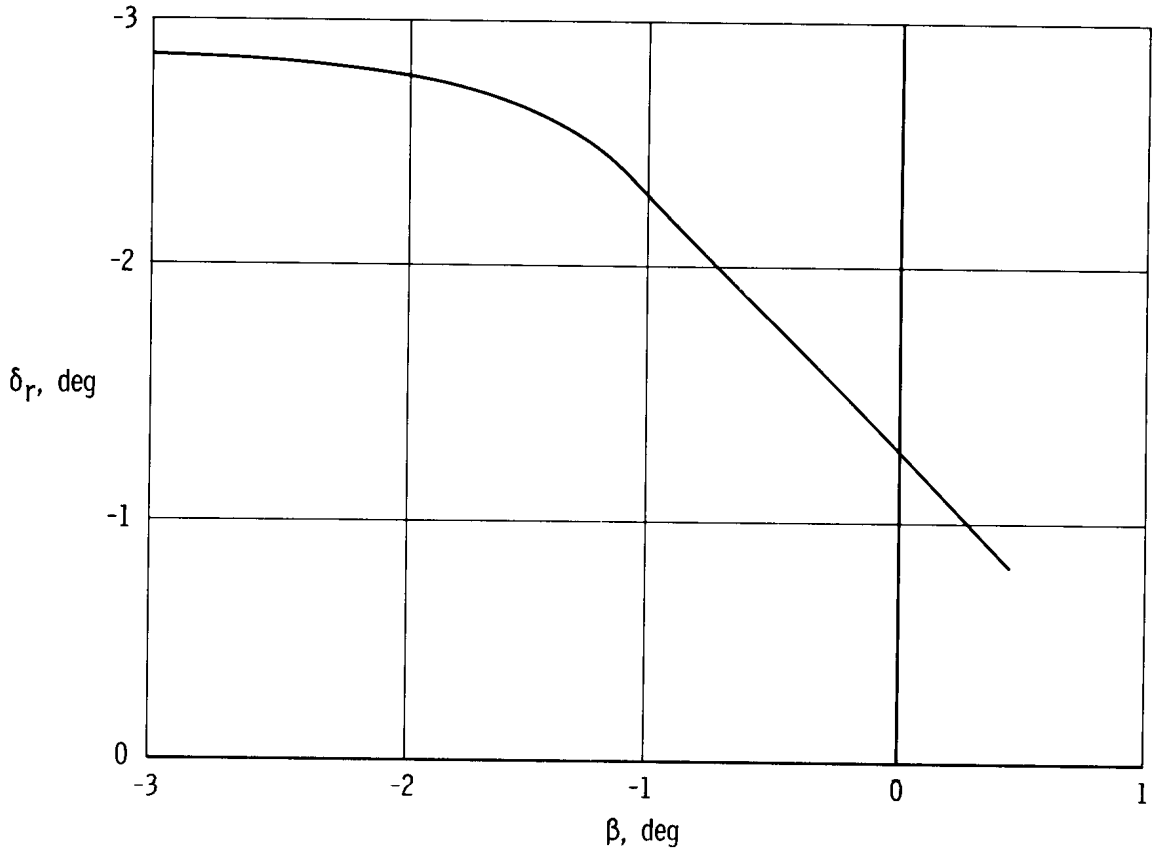

(b) β as a function of δ_r.

Figure 16. Concluded.

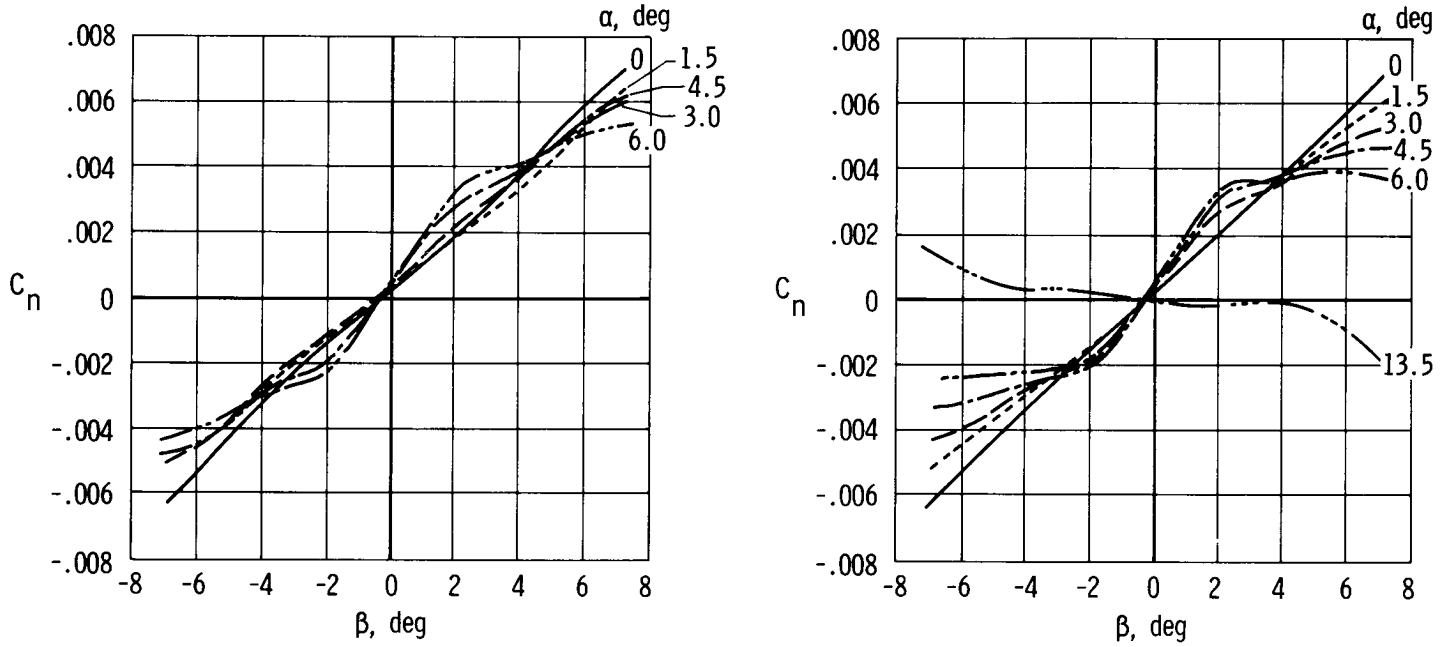

(a) M = 0.75.

(b) M = 1.20.

Figure 17. Variation of yawing-moment coefficient with angle of sideslip at M = 0.75 and 1.20 obtained from unpublished wind-tunnel data. $\delta_T = 25°$; center of gravity = $0.25\bar{c}$; $\delta_e = \delta_c = 0°$.

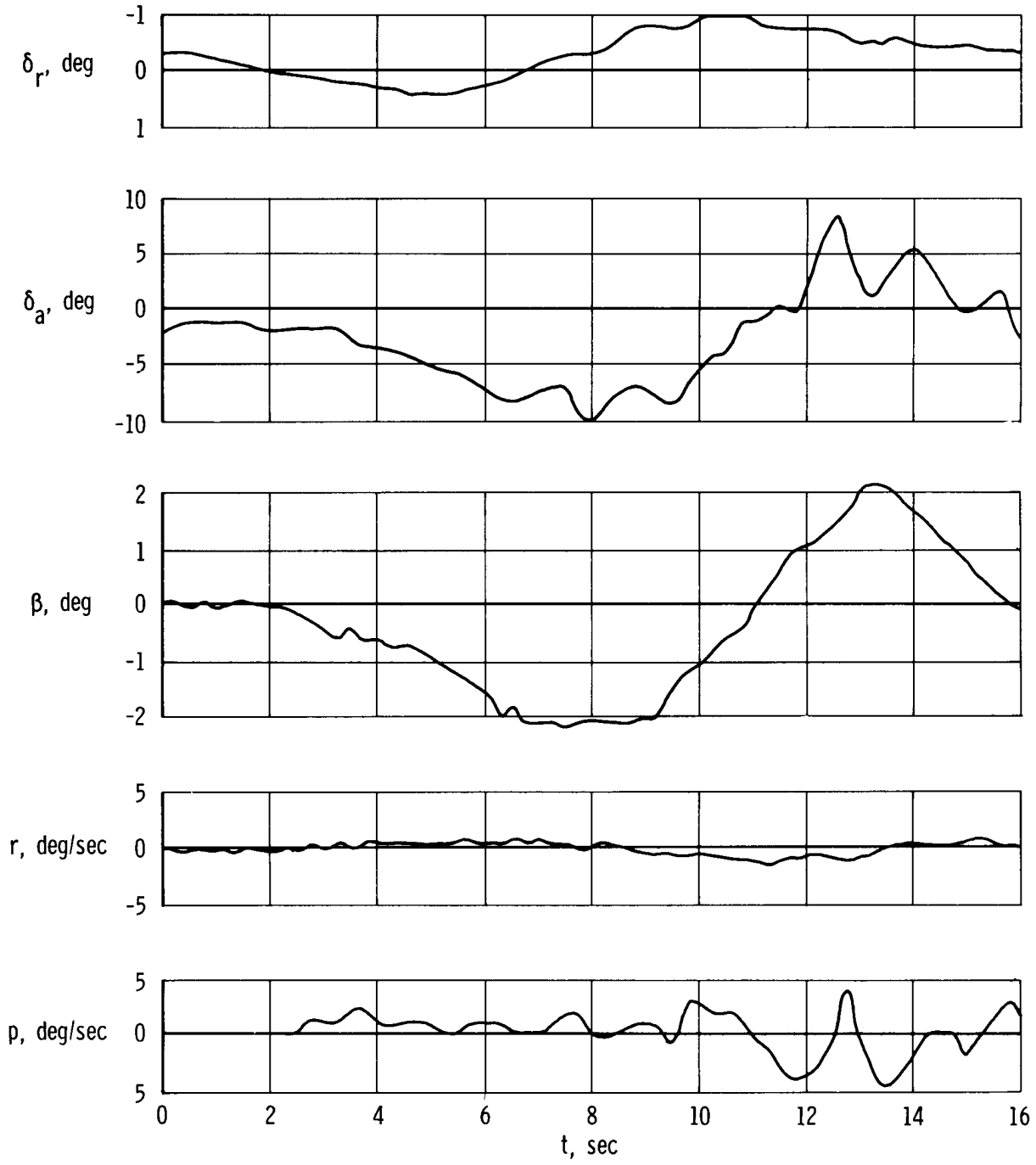

Figure 18. Time history of sideslip maneuver showing effect of adverse aileron yaw. FACS off; $\delta_T = 0°$; M = 1.07; h_p = 10,460 m (34,300 ft); W = 1,581,300 N (355,500 lb); center of gravity = $0.225\bar{c}$; $\delta_e = 7.8°$; $\alpha = 3.6°$.

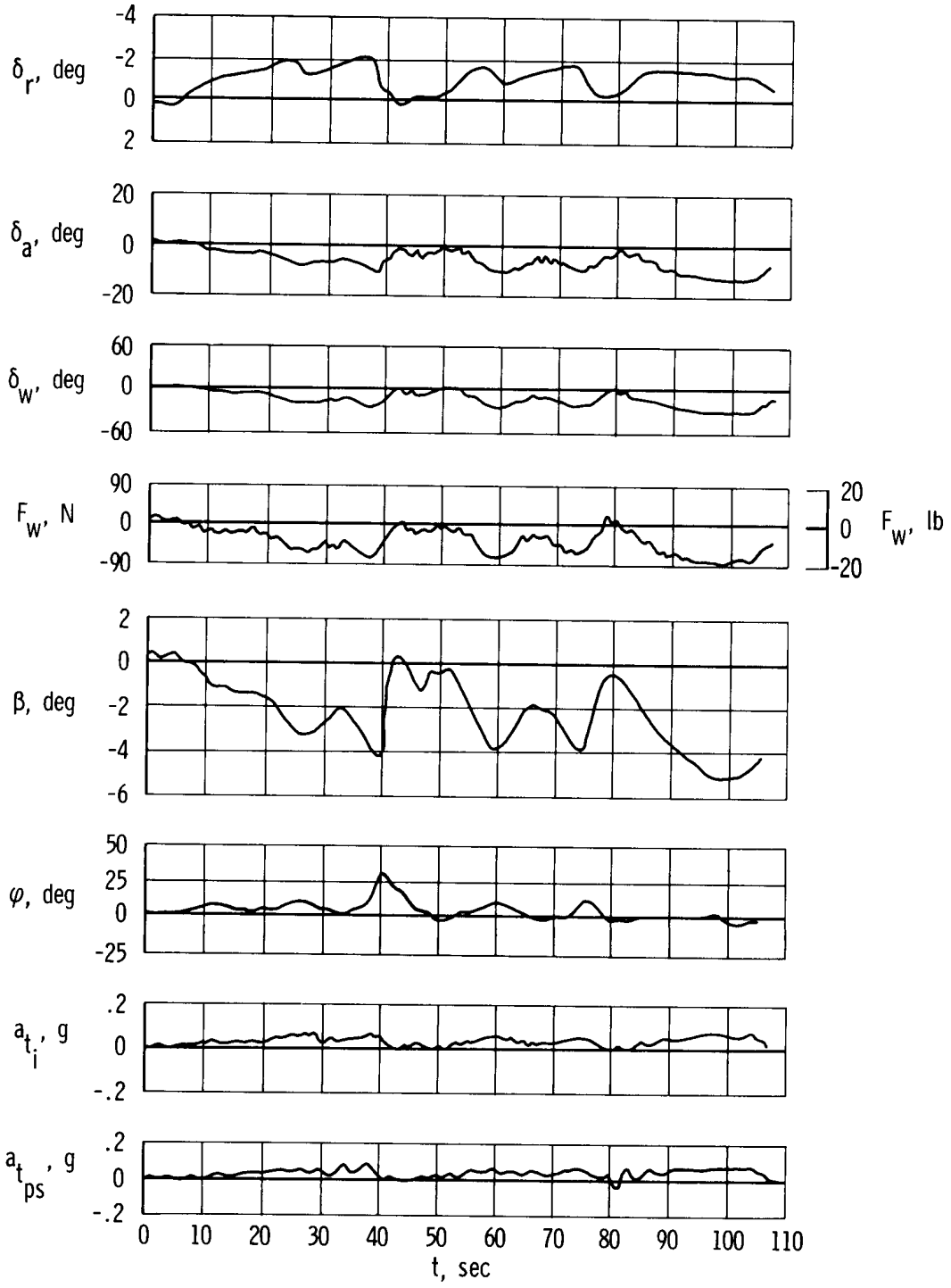

Figure 19. Time history of XB-70-2 sideslip maneuver showing effects of decrease in the static directional stability derivative at sideslip angles above 1.5°; negative aileron yaw; FACS off; M = 0.94; h_p = 10,990 m (36,500 ft); W = 1,325,600 N (298,000 lb); center of gravity = 0.232$\bar{c}$; δ_e = 2.0°; δ_T = 0°; α = 3.5°.

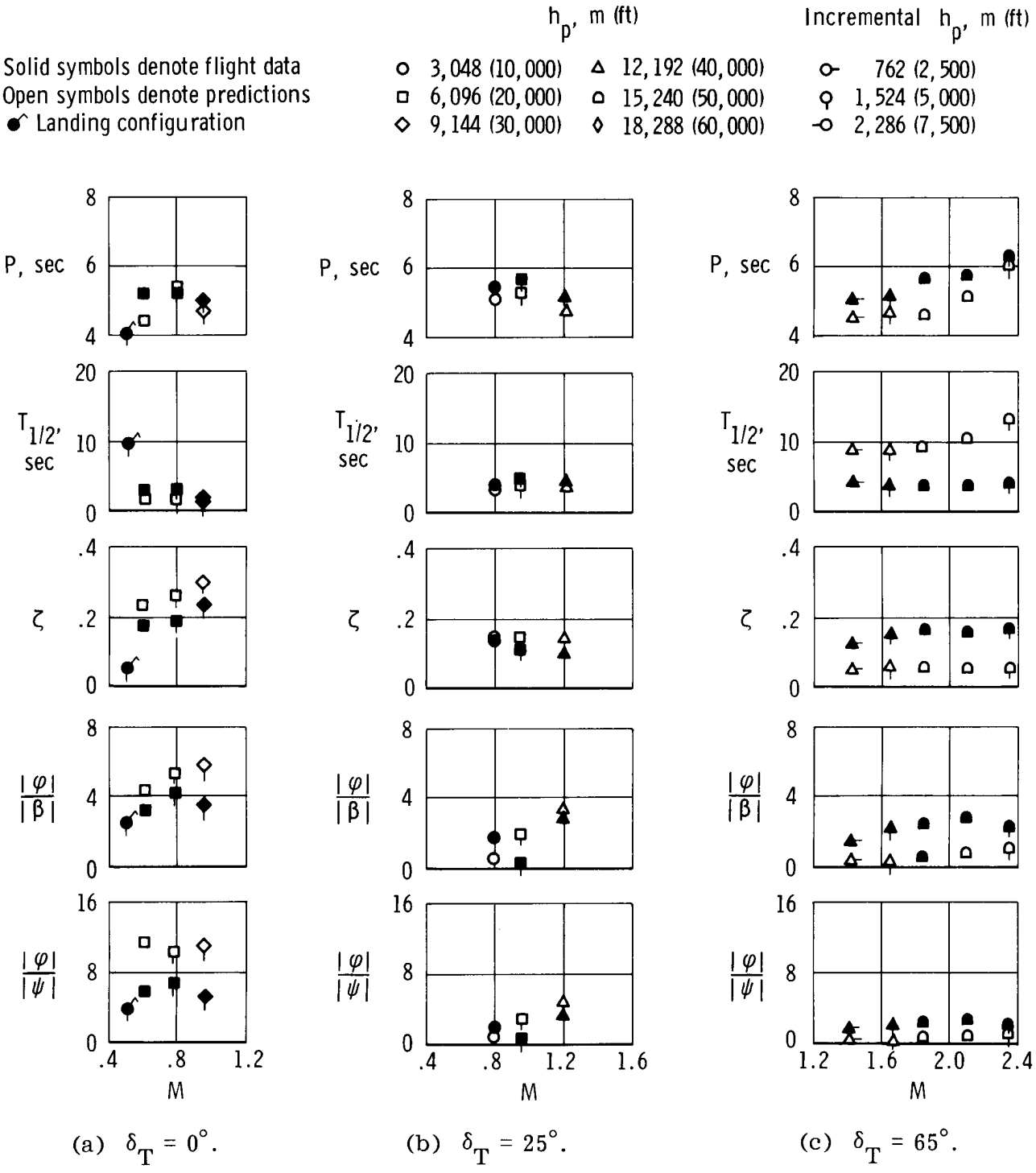

Figure 20. Comparison of flight-determined and predicted Dutch-roll characteristics (from ref. 1). FACS off. Test conditions for individual data points listed in table 5.

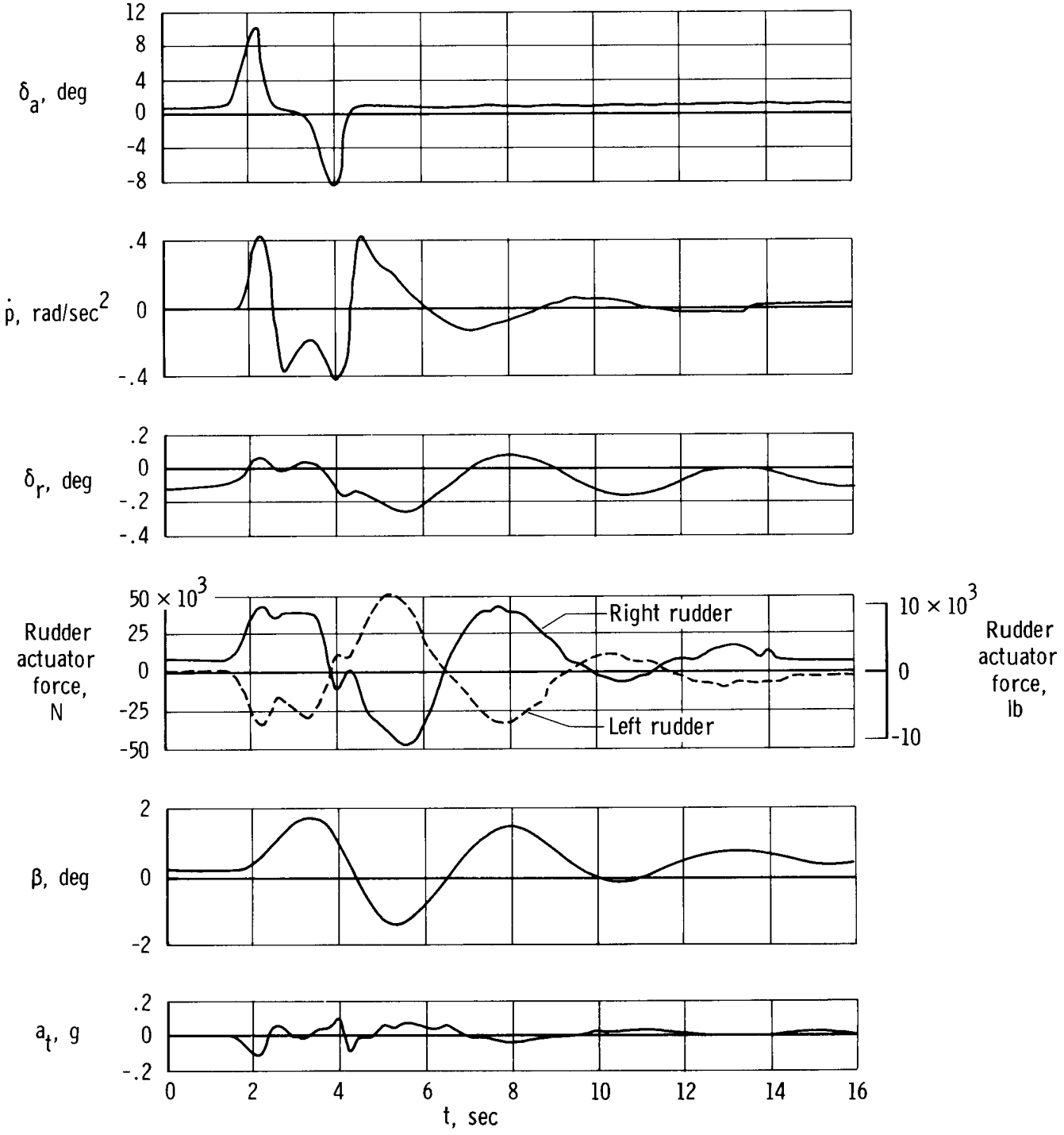

Figure 21. Time history of aileron doublet maneuver showing response of rudder actuator force and rudder to roll acceleration and angle of sideslip. $\delta_T = 0°$; M = 0.74; h_p = 7560 m (24,800 ft).

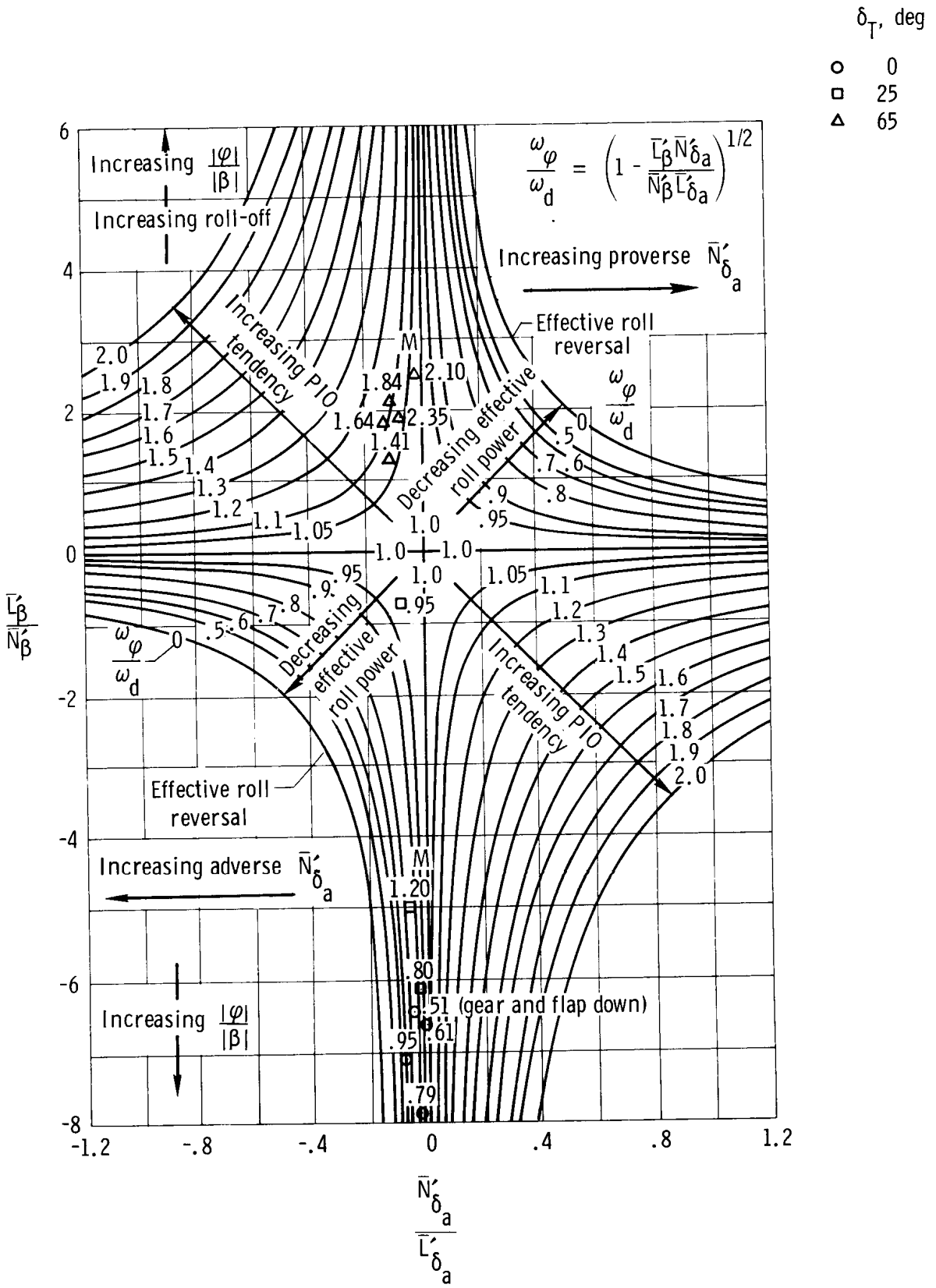

Figure 22. Nomograph giving qualitative insight into the variation with flight condition of the dynamic response to aileron control. FACS off.

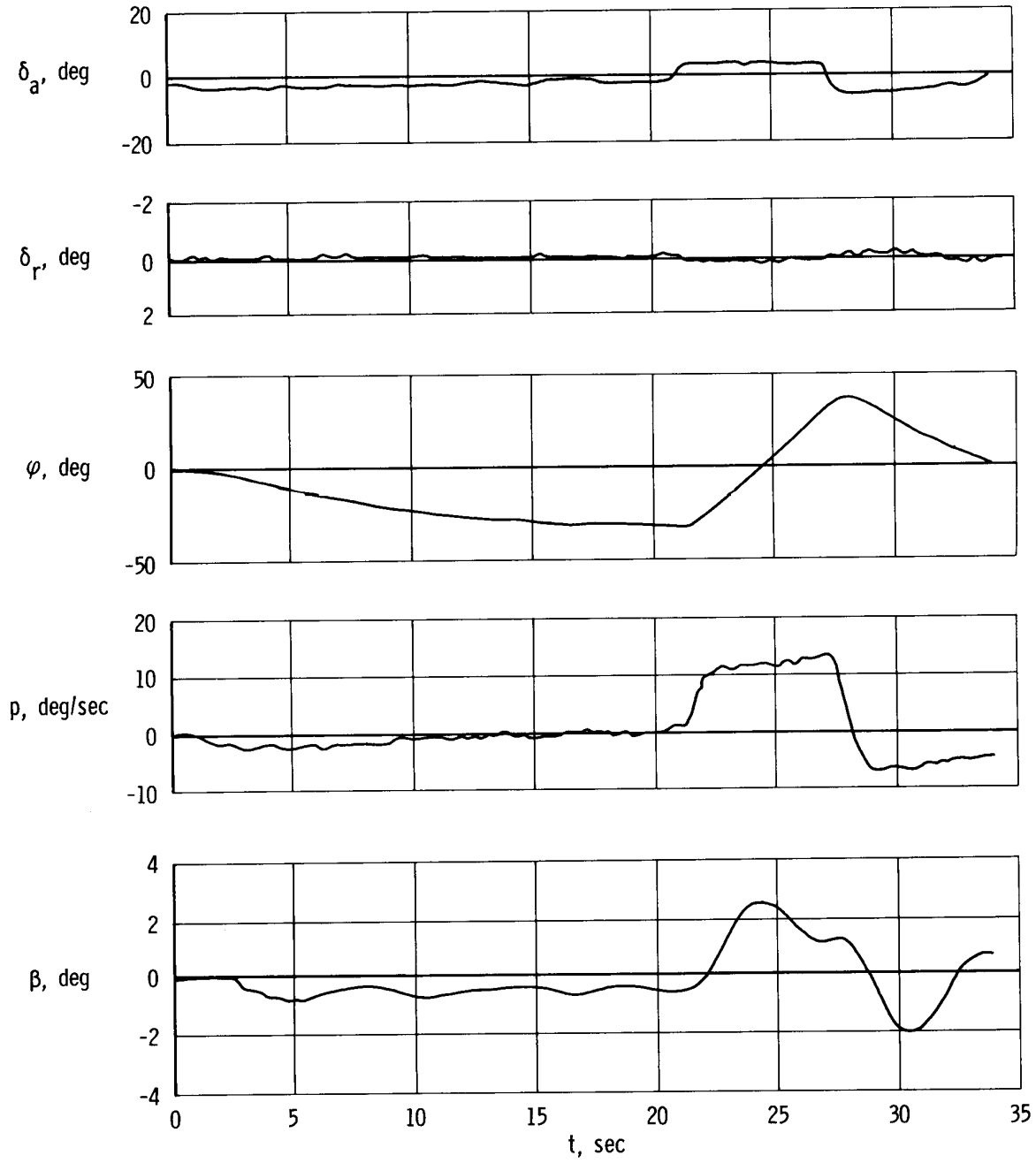

Figure 23. Time history of a 30° turn with a 6.5° aileron rollout from a 30° bank. FACS off; δ_T = 25°; M = 0.79; h_p = 7440 m (24,400 ft); W = 1,467,900 N (330,000 lb); center of gravity = 0.226$\bar{c}$; δ_e = 2.5°; α = 4.5°.

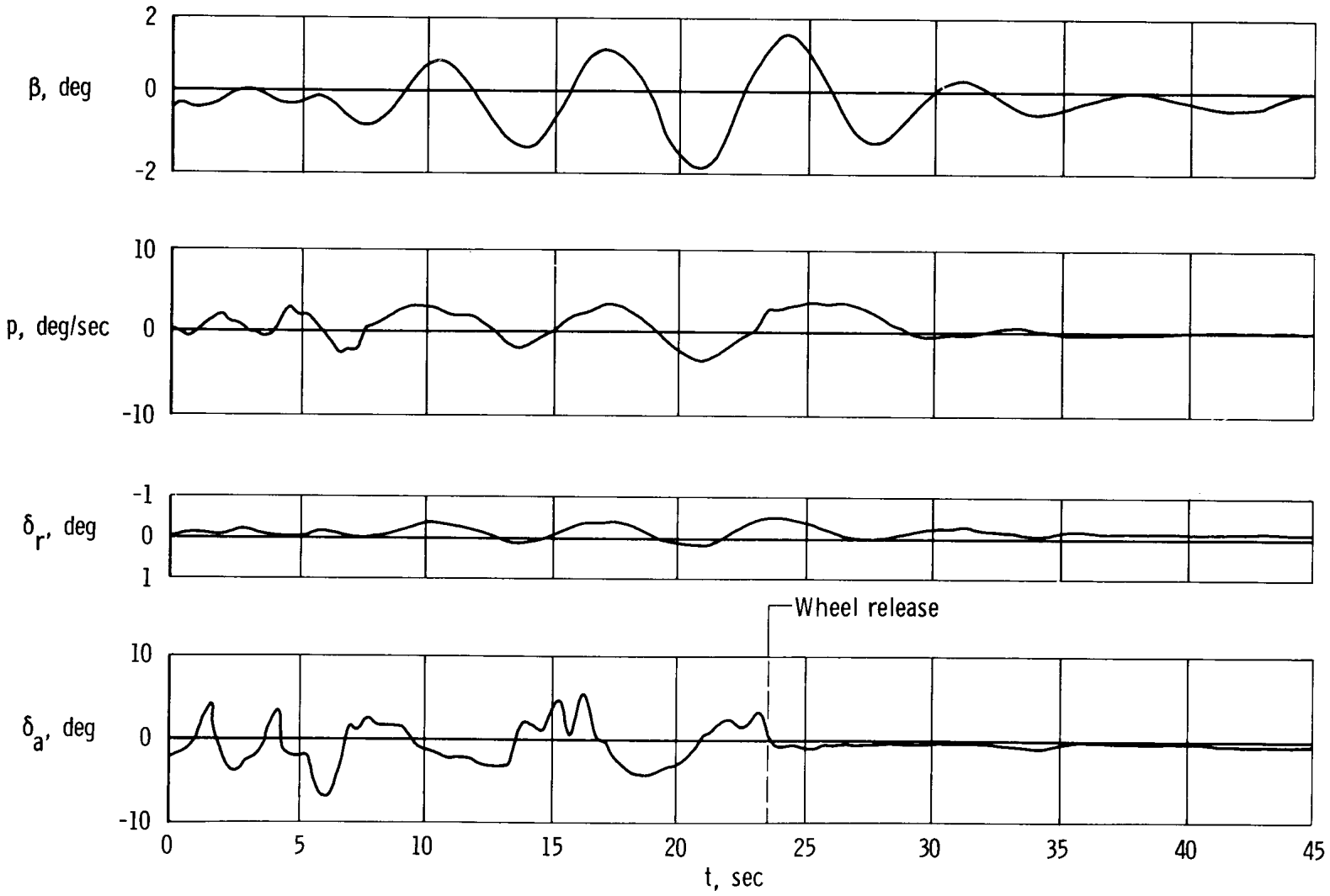

Figure 24. Time history showing pilot-induced oscillation with recovery by means of wheel release. FACS off; $\delta_T = 65°$; M = 2.51; h_p = 18,800 m (61,900 ft); W = 1,668,100 N (375,000 lb); center of gravity = $0.213\bar{c}$; $\delta_e = 1.7°$; $\alpha = 3.5°$.

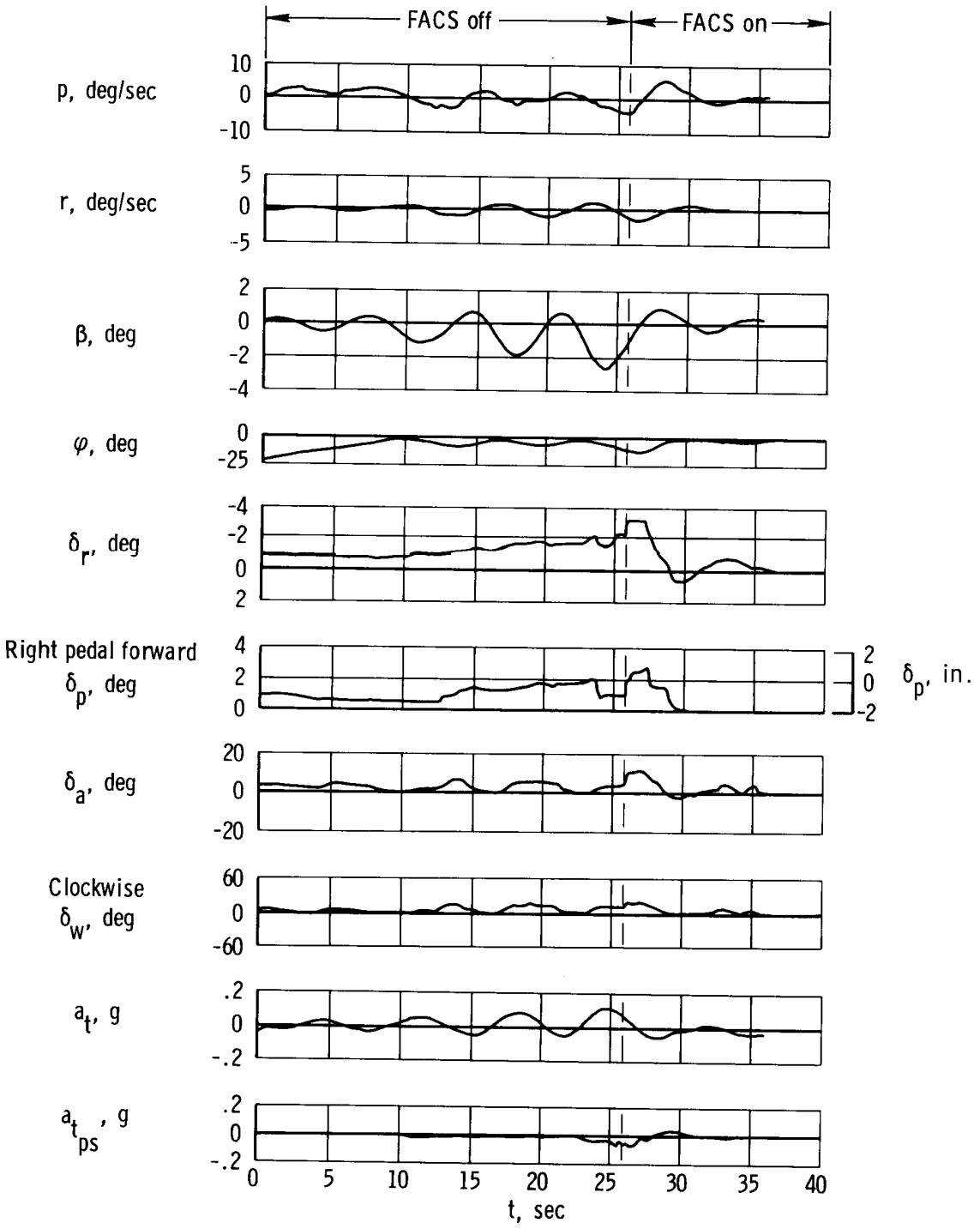

Figure 25. Effect of FACS in damping pilot-induced divergent lateral-directional oscillation during FACS-off recovery from rolloff experienced during transient portion of pullup and release maneuver. δ_T = 65°; M = 2.5; h_p = 18,300 m (60,000 ft); W = 1,694,800 N (381,000 lb); center of gravity = 0.220$\bar{c}$; δ_e = 5°; α = 4°; lateral bobweight locked.

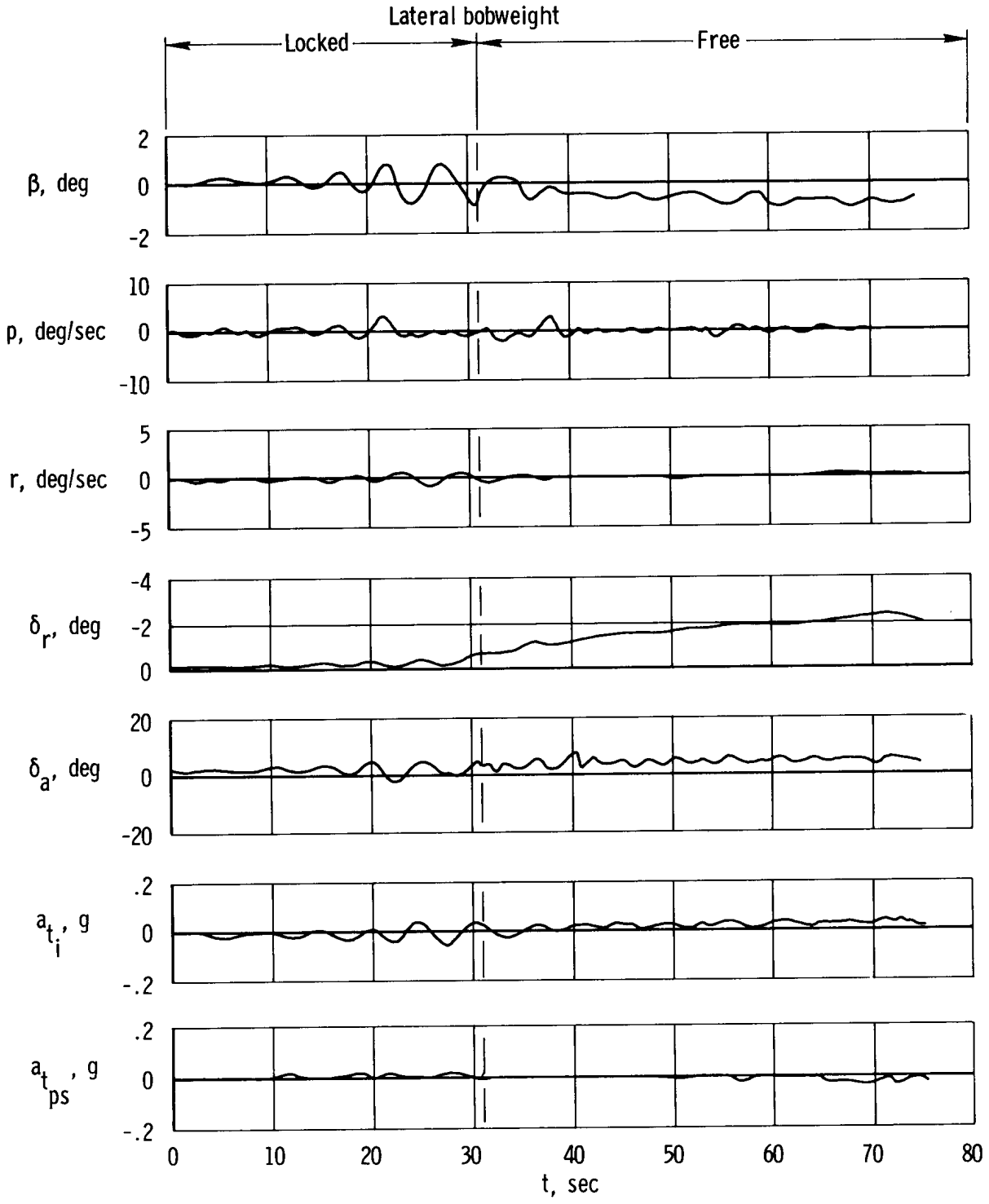

Figure 26. Effect of lateral bobweight in damping a pilot-induced divergent Dutch-roll oscillation during FACS-off sideslip maneuver. $\delta_T = 65°$; M = 2.51; h_p = 18,320 m (60,100 ft); W = 1,594,600 N (358,500 lb); center of gravity = $0.219\bar{c}$; $\delta_e = 5.6°$; $\alpha = 4.0°$.